Polarity of varicosity initiation in central neuron mechanosensation

Yuanzheng Gu,[1] Peter Jukkola,[2] Qian Wang,[3] Thomas Esparza,[4] Yi Zhao,[3] David Brody,[4] and Chen Gu[1,2]

[1]Department of Biological Chemistry and Pharmacology, [2]Biomedical Sciences Graduate Program, and [3]Biomedical Engineering Department, The Ohio State University, Columbus, OH
[4]Department of Neurology, Washington University, St. Louis, MO

Little is known about mechanical regulation of morphological and functional polarity of central neurons. In this study, we report that mechanical stress specifically induces varicosities in the axons but not the dendrites of central neurons by activating TRPV4, a Ca^{2+}/Na^{+}-permeable mechanosensitive channel. This process is unexpectedly rapid and reversible, consistent with the formation of axonal varicosities in vivo induced by mechanical impact in a mouse model of mild traumatic brain injury. In contrast, prolonged stimulation of glutamate receptors induces varicosities in dendrites but not in axons. We further show that axonal varicosities are induced by persistent Ca^{2+} increase, disassembled microtubules (MTs), and subsequently reversible disruption of axonal transport, and are regulated by stable tubulin-only polypeptide, an MT-associated protein. Finally, axonal varicosity initiation can trigger action potentials to antidromically propagate to the soma in retrograde signaling. Therefore, our study demonstrates a new feature of neuronal polarity: axons and dendrites preferentially respond to physical and chemical stresses, respectively.

Introduction

Neurons are highly polarized cells and typically contain multiple dendrites and a single long axon, crucial for conveying input and output electrical signals, respectively. Intrinsic mechanisms governing neuronal polarity have been extensively investigated (Namba et al., 2015; Bentley and Banker, 2016). However, a neuron cannot survive and properly function alone. Besides chemical and electrical communications, it physically interacts with its microenvironment constantly. The interaction depends on the forces acting on and exerted by the neuron, their mechanical properties, and coupling. Although it is widely accepted that mechanical forces are involved in normal neural development, such as neurogenesis, neuron–glia interactions, neuronal migration, axonal outgrowth, growth cone motility, synapse and neural circuit formation, and brain folding (Van Essen, 1997; Gilmour et al., 2004; Engler et al., 2006; Lu et al., 2006; Elkin et al., 2007; Franze et al., 2009; Betz et al., 2011; Amack and Manning, 2012; Cámpas et al., 2014), the underlying mechanisms are poorly understood. In particular, little is known about mechanical regulation of morphological and functional polarity of central neurons. Such possible regulation may represent a novel form of neuronal plasticity.

Mechanical impact can alter the morphology and function of neurons in the central nervous system (CNS). A traumatic brain injury (TBI) includes the primary injury that occurs at the moment of traumatic impact and the secondary injury that occurs afterward and often involves excitotoxicity and inflammation. For neurons, both axons and dendrites are found to be damaged in a TBI. As a prominent feature of TBI, a diffuse axonal injury displays characteristic axonal varicosities (swelling or beading; Smith et al., 2013). In mild TBI (mTBI), axons are not uniformly injured, and unmyelinated axons appear more vulnerable (Reeves et al., 2005). On the other hand, dendritic varicosities and degenerating spines were also observed in the mTBI mouse model (Gao et al., 2011). However, it is not clear which neuronal compartment is more likely damaged first during the initial primary injury. Moreover, abundant axonal varicosities are a key sign for irreversible neurodegeneration in Alzheimer's and Parkinson's diseases and multiple sclerosis (Nikić et al., 2011; Yang et al., 2013). In fact, even in the normal CNS, not all axons appear like perfect long tubes with uniform diameters. Axonal varicosities often form before axonal pruning and synapse formation during development of the CNS and persist at a low level in the normal adult brain (Shepherd and Harris, 1998; Luo and O'Leary, 2005; Nikić et al., 2011; Smith et al., 2013). Although varicosities can profoundly affect action potential propagation and synaptic transmission (Debanne, 2004), how varicosities are induced in axons under various normal and abnormal conditions remains a mystery.

Correspondence to Chen Gu: gu.49@osu.edu

Abbreviations used: AIS, axon initial segment; AM, acetoxymethyl; CNS, central nervous system; DIV, day in vitro; MBP, myelin basic protein; MS, mechanosensitive; MT, microtubule; mTBI, mild TBI; NMDA, *N*-methyl-D-aspartate; NMDG, *N*-methyl-D-glucamine; STOP, stable tubulin-only polypeptide; TBI, traumatic brain injury; TEM, transmission EM; TRP, transient receptor potential; TTX, tetrodotoxin.

The Rockefeller University Press
J. Cell Biol. Vol. 216 No. 7 2179–2199
https://doi.org/10.1083/jcb.201606065

It is not known how micromechanical stress regulates axonal varicosity formation in terms of time course, reversibility, and underlying mechanism. Because the vertebrate brain is well protected by the skull, its structure and function have not been extensively investigated in the context of mechanics. The investigation is further hindered in part by technical challenges in microbiomechanical measurements and manipulations as well as a knowledge gap in mechanosensitive (MS) proteins and their downstream signaling pathways.

Progress has been made in understanding mechanosensation and mechanotransduction of specialized cell types and organs, such as cochlear hair cells, touch-sensing organs in skin, and kidneys for fluid pressure, where MS ion channels play critical roles in rapid sensing and responding to mechanical stimuli (Árnadóttir and Chalfie, 2010; Delmas et al., 2011). Newly identified MS channels are emerging rapidly, including some that are traditionally assigned for completely different functions (Gu and Gu, 2014). Several criteria are suggested to define an MS ion channel, including tissue expression, deletion phenotype, in vitro reconstitution, and the mechanosensing mechanism of the channel (Christensen and Corey, 2007; Árnadóttir and Chalfie, 2010). So far, only a few candidates meet all these criteria (Gu and Gu, 2014). Several members of the transient receptor potential (TRP) channel family represent a major group among MS ion channels. The first TRP channel was described in the fruit fly *Drosophila melanogaster* in 1969 and was later cloned in 1989 (Cosens and Manning, 1969; Montell and Rubin, 1989). All TRP channel members can be divided into eight subfamilies (TRPC, TRPV, TRPM, TRPN, TRPA, TRPP, TRPML, and TRPY in yeast; Venkatachalam and Montell, 2007). These channels can be activated by light, sound, chemicals, temperature, osmolarity, touch, heat, the phorbol ester derivative, or lipids downstream of arachidonic acid metabolism. It appears that nearly every TRP subfamily contains a member that can be activated by physical stimuli (Christensen and Corey, 2007). The TRPV subfamily contains six members (TRPV1–TRPV6). Its first member, TRPV1, the capsaicin receptor, was cloned in 1997 (Caterina et al., 1997). TRPV4, first cloned in 2000, is also known as vanilloid receptor–related osmotically activated channel (VR-OAC), OTRPC4, TRP12, or VRL-2 (Liedtke et al., 2000; Strotmann et al., 2000). Both TRPV1 and TRPV4 are candidates of MS ion channels (Liedtke and Friedman, 2003; Venkatachalam and Montell, 2007; Gu and Gu, 2014). However, the potential roles of MS TRP channels in the CNS are underexplored and are thus still poorly understood.

Signaling downstream to mechanical activation during injury is still not clear, especially in axonal varicosity formation. A recent study shows that axonal injuries induce axon–soma communication through the following two mechanisms: a rapid one encoded by Ca^{2+} waves and a slower one conveyed by molecular motors (Rishal and Fainzilber, 2014). In axotomy, the breach of the axonal membrane causes rapid changes in intracellular ion concentrations via Ca^{2+} channel activation, reversal of the Na^{+}/Ca^{2+} exchanger, and/or Ca^{2+} release from internal stores, inducing Ca^{2+} waves propagating back to the soma (Ziv and Spira, 1995; Cho et al., 2013). The slower retrograde signaling is mediated by macromolecular signaling complexes that are carried by dynein motors, a mechanism likely shared with retrograde neurotrophic factor signaling and subjected to complex regulations (Harrington and Ginty, 2013; Rishal and Fainzilber, 2014). Therefore, it will be interesting to determine whether and how axons may rapidly communicate with the soma under micromechanical stress.

In this study, we discovered that mechanical stress preferentially induces varicosities in the axons of hippocampal neurons. In sharp contrast, excitotoxicity induces varicosity formation in the dendrites. Mechanical stress–induced varicosity formation in axons is unexpectedly rapid and reversible. Our study further reveals that an MS ion channel (TRPV4) and a microtubule (MT)-binding protein (stable tubulin-only polypeptide [STOP]) play critical roles in this process. Importantly, varicosity initiation in axons can trigger action potentials to antidromically propagate to the soma as a novel rapid form of retrograde communication. These results provide new mechanistic insights into axonal varicosity initiation, a novel form of neuronal plasticity and a potentially common process in both normal neural development and subconcussive brain injury.

Results

Micromechanical stress induces rapid and reversible formation of varicosities in the axons but not the dendrites of central neurons

To visualize axonal and dendritic morphology in different CNS regions, we imaged brain sections expressing YFP from Thy1-YFP transgenic mice in which a subset of projection neurons expresses YFP. Although neuronal morphology was clearly revealed by YFP fluorescence, we stained myelin segments with an antibody against myelin basic protein (MBP), a mature myelin marker. We found axonal varicosities that were indicated by YFP along unmyelinated but not myelinated axons in the hippocampus as well as in other brain regions (Fig. 1 A). In sharp contrast, varicosities were never found along dendrites in the normal brain. Our results are consistent with a previous study showing that many axonal varicosities in the hippocampal CA3 region are likely presynaptic boutons, whereas some do not contain any presynaptic apparatuses and hence have unknown function (Shepherd and Harris, 1998). We were intrigued by this observation and wondered why axonal varicosities are present in unmyelinated axons but not in dendrites and myelinated axons. Furthermore, how are axonal varicosities initiated and maintained in general? Do they represent irreversibly degenerating axons like those observed in injured or diseased brains?

In a drug perfusion experiment, we accidentally discovered that puffing Hank's buffer itself induced rapid and reversible varicosity formation along axons of cultured hippocampal neurons (Fig. 1 B and Video 1). The solution in the puffing pipette was identical to the bath solution (Hank's buffer) and was driven by gravity; axonal varicosity formation correlated with the strength of puffing pressure (Fig. S1, A and B). To determine whether the puffing pressure was within the ranges of physiological and pathophysiological conditions in the brain, we measured and compared it with other known values of micromechanical pressure. Although the static pressure at the tip of the puffing pipette can be calculated, the exact fluid pressure onto the neurons had to be determined experimentally. When 190 mmH_2O static pressure (at the tip) was applied via the puffing pipette, there was ∼0.25 ± 0.06 $nN/\mu m^2$ pressure on the neurons, which was measured with microfabricated silicone membranes as described previously (Fig. S1 C; Wang et al., 2013). This value (including both compression and shear)

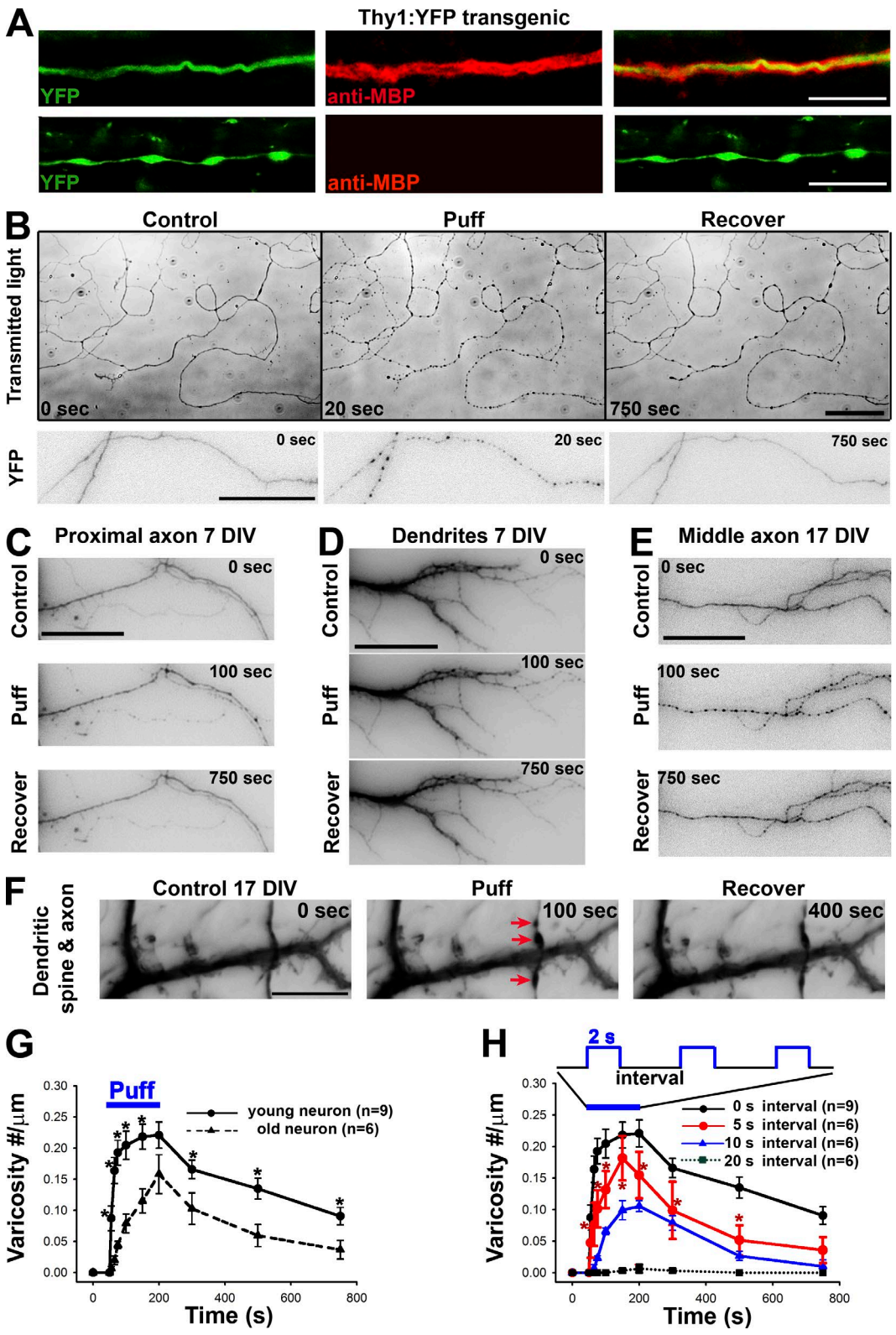

Figure 1. **Mechanics-induced rapid and reversible initiation of axonal varicosities.** (A) Axonal varicosities along unmyelinated (bottom) but not myelinated axons (top) in the hippocampus of Thy1-YFP transgenic mice. Axons are indicated by YFP fluorescence (green) and myelin segments by the anti-MBP staining (red). (B) Puffing induced rapid and reversible formation of axonal varicosities in cultured hippocampal neurons at 7 DIV, revealed by transmitted lights (top) and transiently expressed YFP (bottom). YFP signals are inverted. Transient or sustained mechanical pressures were delivered by puffing of Hank's buffer via a glass pipette onto cultured hippocampal neurons as described in Fig. S1. The puffing time was 150 s. (C) Puffing did not induce varicosity formation in proximal axons (7 DIV). Neurons were transfected with YFP. The soma was on the left. (D) Puffing did not affect dendrite morphology (7 DIV). (E) Puffing induced varicosity formation in the middle axon of a neuron at 17 DIV. (F) Puffing induced varicosity formation along axons but not dendrites nor

is physiologically and/or pathologically relevant, which will be discussed in the Discussion. Our experimental setting may mimic increased local mechanical stress onto unmyelinated CNS axons induced by cell growth and migration, tissue swelling, or mechanical impact. Throughout the rest of study, 190 mmH_2O was used for puffing for reliably inducing axonal varicosities, whereas 50 mmH_2O was used for perfusion, under which no varicosity could form.

To determine the spatial and temporal specificity of hippocampal neuron mechanosensation, we first examined how puffing affected different neuronal compartments. Puffing only induced varicosities along middle and distal axons, but not in dendrites, dendritic spines, or proximal axons (Fig. 1, C–F; Fig. S2 A; and Video 2). Axonal varicosities were highly restricted within the axonal segment inside the puffing area (Fig. S2 B). During puffing, varicosity initiation was much faster in young axons (~7 d in vitro [DIV]) than older ones (~21 DIV), but importantly, both types of axons started to recover right after puffing (Figs. 1 G and S2, C and D). This rapid, reversible, and localized change of axonal morphology in response to micromechanical stress may represent a previously unrecognized form of neuronal plasticity, different from axon degeneration.

To investigate how varicosity initiation may be regulated by trains of short puffing pulses, which mimic repetitive subconcussive impacts, we applied short puffing pulses (2 s in duration) at different frequencies. Axonal varicosities were induced in a frequency-dependent manner. No obvious varicosity formation was observed if the interval was at or longer than 20 s, but at 5-s intervals, varicosities were rapidly induced (Fig. 1 H). Thus, there is a clear accumulative effect of short pulses of micromechanical stress on central neuron axons.

Formation of axonal varicosities in the mouse model of repetitive closed-skull TBIs

To confirm the in vivo relevance of puffing-induced formation of axonal varicosities, we performed the mouse model of repetitive closed-skull TBIs (Shitaka et al., 2011). Thy1-YFP transgenic mice were used for analyzing morphological changes of the axons and dendrites of a subset of projection neurons immediately after the second impact. This early time point was not examined before. In this experiment, we focused on examining varicosity formation in YFP^+ axons and dendrites in the somatosensory cortex, which was directly beneath the impact site and hence the primary region of injury in which mechanical forces were presumably the highest (Fig. 2 A). Indeed, many axonal varicosities were observed together with apparently normal dendrites nearby in a multifocal fashion in mTBI mice (Fig. 2, B and C). These varicosities resemble to those in cultured neurons induced by puffing in terms of the size, number, and pattern (Fig. 2, D and E). To determine whether some of these varicosities in mTBI mice might be presynaptic boutons, we performed costaining for two different endogenous markers of presynaptic boutons: Bassoon and vesicle-associated membrane protein 2 (VAMP2). We found that the majority of these varicosities in mTBI mice did not contain the two presynaptic markers (Fig. 2, F–I). Thus, most of these varicosities induced in mTBI mice are not likely presynaptic boutons. Collectively, this experimental result confirmed that axonal varicosities indeed rapidly form upon mechanical impact in vivo in the mouse model of repetitive mTBI.

TRPV4 is the major MS ion channel mediating puffing-induced axonal varicosity formation in hippocampal neurons

The new features of puffing-induced formation of axonal varicosities include rapid onset, slow reversibility, and localized and cumulative properties (Figs. 1 and S2), suggesting a role of ionic influx through MS ion channels on axonal membranes. To determine which cation in Hank's buffer is required for puffing-induced varicosity initiation in axons, we replaced three cations one by one in the buffer. In puffing experiments, the bath and pipette solutions were always identical. Removing Ca^{2+} but not Mg^{2+} significantly increased the time for varicosity formation and reduced varicosity size and abundance (Fig. S3, A–D). Interestingly, replacing Na^+ with *N*-methyl-D-glucamine (NMDG), an organic monovalent cation, also made axons more resistant to puffing, but its effect was significantly less than that of removing Ca^{2+}, especially in onset time and varicosity density (Fig. S3, A–D). The most effective condition to suppress puffing-induced varicosity initiation was removal of both Ca^{2+} and Na^+ (Fig. S3, A–D; Videos 3 and 4). These results indicate that Ca^{2+} influx plays a major role in puffing-induced varicosity initiation, whereas Na^+ influx may play a minor role. Therefore, the MS channels involved in puffing-induced varicosity formation in axons are likely permeable to Ca^{2+} and, to a lesser extent, Na^+.

Among the known MS ion channels (Gu and Gu, 2014), we focused on TRPV1 and TRPV4 because they are permeable to Ca^{2+} and, to a lesser extent, Na^+ and are present in central neurons (Shibasaki et al., 2007; Gibson et al., 2008). In particular, the ratio of Ca^{2+} and Na^+ permeability of TRPV4 is ~6:1. When being perfused, the TRPV4 agonist (0.1 µM GSK101) was significantly more effective than the TRPV1 agonist (1 µM capsaicin) in inducing axonal varicosities (Fig. S3, E–G). Conversely, treating with Gd^{3+} (200 µM; a general blocker for MS ion channels), RN1734 (10 µM; a TRPV4-specific blocker), or HC067047 (100 nM; another TRPV4-specific blocker) markedly reduced puffing-induced varicosities (Fig. S3, E–G), suggesting a potential role of TRPV4 in this process.

To recapitulate the mechanosensation, we expressed TRPV1 and TRPV4 channels in HEK293 cells and performed whole-cell voltage-clamp recording. Both channels were activated by their respective agonists, but only TRPV4 was activated by puffing that could induce axonal varicosities (Fig. 3, A–C). To determine TRPV4 expression and targeting in hippocampal neurons, we used an antibody against TRPV4 that was previously extensively validated (Ryskamp et al., 2011). TRPV4 was indeed expressed in cultured hippocampal neurons with relatively higher axonal levels in young neurons, whereas its axonal level moderately declined in mature neurons (Fig. S4). To estimate TRPV4 levels at the axons that are sensitive to mechanical stress, we performed the puffing experiment on hippocampal neurons (6 DIV) loaded with calcein acetoxymethyl (AM) dye and fixed the

dendritic spines at 17 DIV. Red arrows indicate axonal varicosities. Related quantifications are included in Fig. S2. Bars: (A) 10 µm; (B) 50 µm; (C–F) 15 µm. (G) Older axons (21 DIV) were more resistant to puffing-induced varicosity formation than younger ones (7 DIV). (H) Frequency-dependent varicosity initiation in young axons receiving 2-s puffing pulses. Error bars show means ± SEM. Unpaired *t* test: *, $P < 0.05$. 5-s interval versus 20-s interval in H.

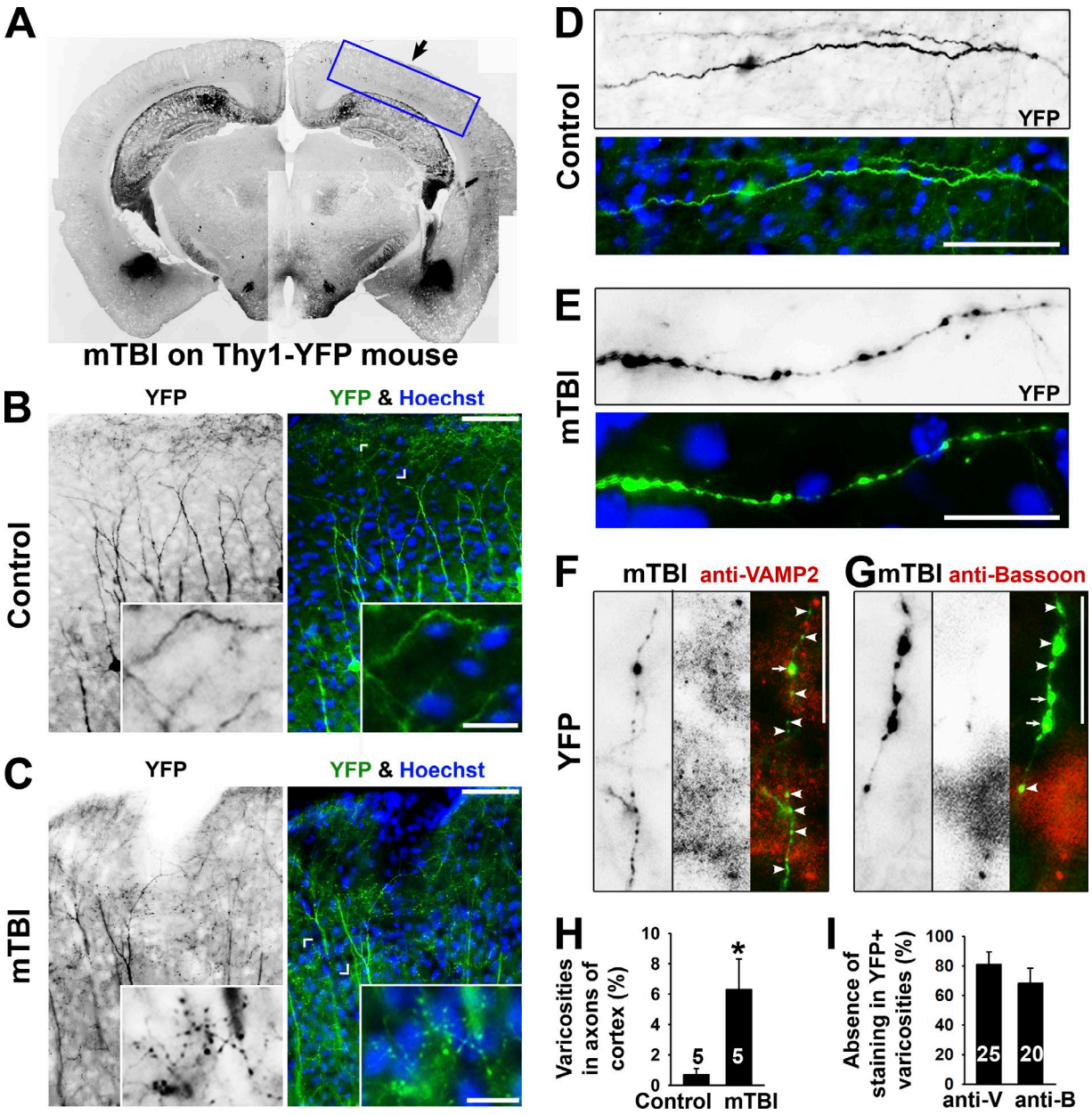

Figure 2. **Axonal varicosity induction in a repetitive closed-skull mTBI mouse model.** (A) Low-magnification image of a coronal section from the brain of a Thy1-YFP transgenic mouse that had received impact on the right side. YFP fluorescent signals are inverted. This is a compilation of multiple images. The boxed area indicates the brain region that this study focused on. The black arrow indicates head impact location. (B) YFP$^+$ dendrites and axons in the cortex of a control mouse. The apical dendrites of layer V projection neurons in the cortex point in the upward direction. (C) YFP$^+$ dendrites and axons in the cortex of an mTBI mouse. Cornered areas are provided in the insets to show normal axons (B) and axons with clear varicosities (C). (D) A normal axonal segment from a control mouse. (E) An axonal segment with many varicosities from an mTBI mouse. YFP is in green, and nuclear dye Hoechst is in blue in merged images. (F and G) Partial colocalization of axonal varicosities (left gray images; green in the merged images) with presynaptic markers (middle gray images; red in the merged images) in VAMP2 (F) and Bassoon (G) from mTBI mice. Arrows indicate axonal varicosities (indicated by YFP) containing a presynaptic marker (indicated by anti-VAMP2 or anti-Bassoon staining), and arrowheads indicate axonal varicosities without presynaptic markers. Bars: (B and C, main images) 100 µm; (B and C, insets) 30 µm; (D–G) 20 µm. (H) Percentages of axons with clear varicosities in control and mTBI mice. (I) Percentages of varicosities in axons from mTBI mice without costaining of the presynaptic markers. Error bars indicate means ± SEM. Unpaired *t* test: *, $P < 0.05$. anti-B, anti-Bassoon; anti-V, anti-VAMP2.

neurons after varicosities were induced. Indeed, distal axons had higher levels of endogenous TRPV4, revealed by post hoc staining, and the most varicosities, revealed by calcien AM fluorescence, induced by puffing (Fig. 3, D–F).

To determine the role of TRPV4 in puffing-induced axonal varicosity initiation, we adopted the siRNA knockdown approach. The siRNA probe was extensively validated and published previously (Benfenati et al., 2011). Transiently knocking down TRPV4 with siRNA significantly increased the onset time and reduced the size of varicosities (Fig. 3, G–J). However, it did not completely eliminate varicosities, consistent with a partial knockdown by siRNA (Fig. 3, K–M). This partial knockdown agrees with previously reported results (Benfenati et al., 2011). Collectively, these results confirmed a major role

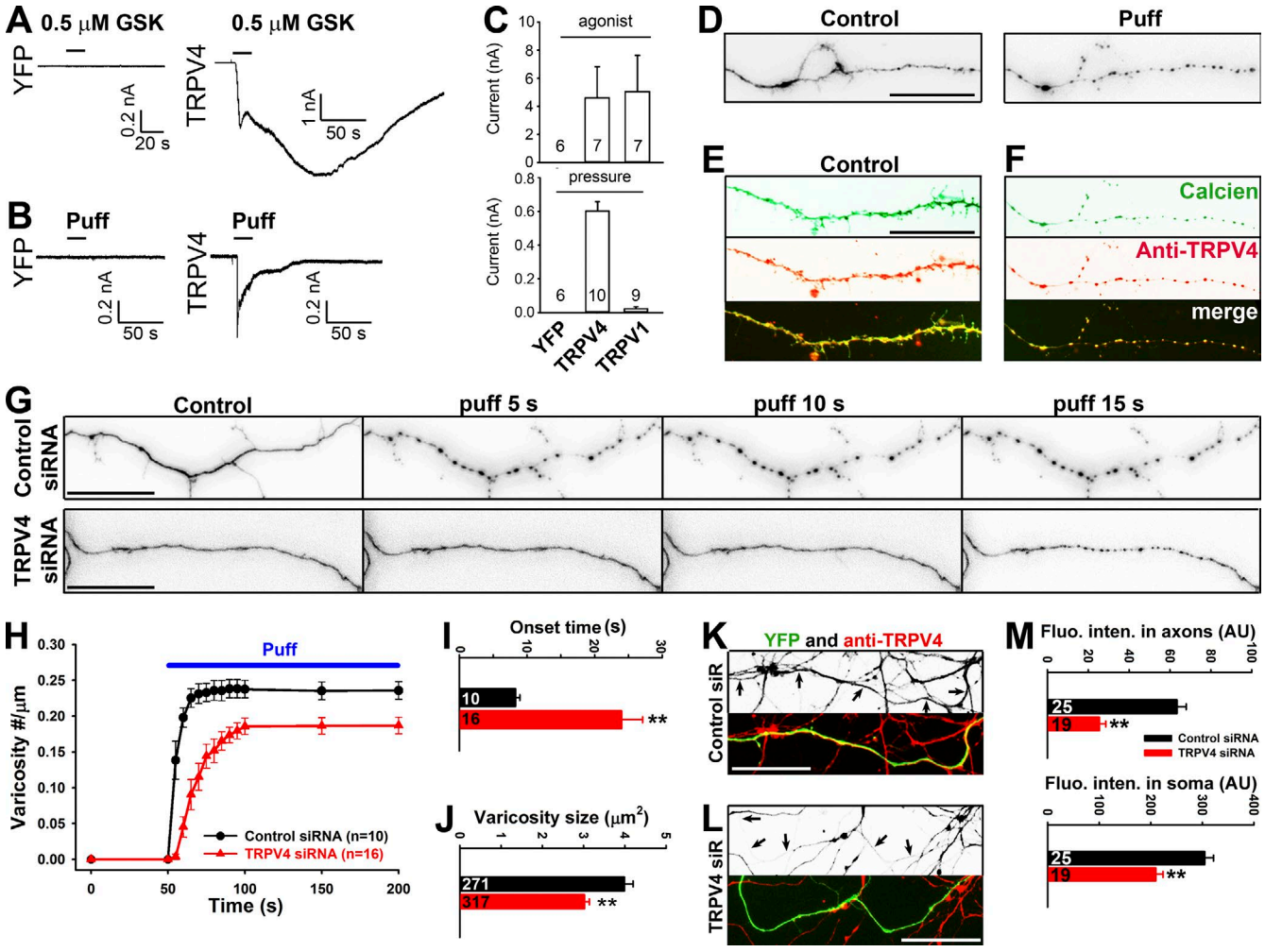

Figure 3. **TRPV4 channel plays a major role in axonal varicosity initiation in hippocampal neuron mechanosensation.** (A and B) When expressed in HEK293 cells, TRPV4 but not YFP was activated by TRPV4 agonist GSK101 (GSK; 0.5 µM; A) and puffing (B). (C) Summary of the effects of their respective agonist (top) or puffing (bottom) on HEK293 cells expressing YFP, TRPV4, or TRPV1. (D) An axonal segment loaded with calcien AM (inverted signals) before (left) and after (right) puffing. (E) A distal axonal segment loaded with calcien AM (green) without puffing and stained for endogenous TRPV4 (red). (F) Post hoc staining of the axon in D for endogenous TRPV4 (red). (G) Effects of puffing on axons transfected with control (top) or TRPV4 (bottom) siRNA (siR). (H) The onset and degree of varicosity formation along axons with TRPV4 siRNA markedly reduced. (I and J) Under the same puffing condition, axons with TRPV4 siRNA had significantly longer onset time (I) and smaller varicosities (J). (K) Young axons (7 DIV) expressing YFP (green) and control siRNA were stained for endogenous TRPV4 (red in merged image and inverted in grayscale image). (L) Young axons (7 DIV) expressing YFP (green) and TRPV4 siRNA were stained for endogenous TRPV4 (red in merged image and inverted in grayscale image). Arrows indicate coexpressing YFP and double-stranded small RNA. Bars, 20 µm. (M) TRPV4 siRNA significantly reduced TRPV4 staining intensity in both axons and soma of cultured neurons. Error bars indicate means ± SEM. Unpaired *t* test: **, $P < 0.01$.

of TRPV4 in axonal varicosity formation that is induced by micromechanical stress.

Opposite polarity of varicosity formation induced by mechanical stress and excitotoxicity

Why does puffing specifically induce varicosity formation in axons but not in dendrites? This may result from a more pronounced TRPV4 activity in axons. TRPV4 channel proteins appear relatively more enriched in distal axons of young neurons, but overall polarized targeting of TRPV4 is not impressive, especially in older neurons (Fig. 3, D–F; and Fig. S4). Therefore, it is possible that signaling downstream to TRPV4 activation also plays a critical role in this polarized mechanosensation. Prolonged increase of intracellular Ca^{2+} can destroy mitochondria, generate reactive oxygen species, and activate proteolytic enzymes to degrade ion channels and cytoskeleton proteins (Iwata et al., 2004; Yang et al., 2013). Calpain is a key Ca^{2+}-activated nonlysosomal protease in axon degeneration, but its action requires long-lasting Ca^{2+} elevation (~30 min) and is irreversible (Iwata et al., 2004; Yang et al., 2013) and therefore unlikely to be responsible for such rapid initiation of axonal varicosities.

To dissect the signaling pathway involved in axonal varicosity initiation, we first compared puffing- and glutamate (Glu)-induced varicosity formation in different neuronal compartments. Prolonged stimulation of the Ca^{2+}-permeable *N*-methyl-D-aspartate (NMDA) receptor was shown to induce swellings in dendrites via MT disassembly, but its effect on axons was unknown (Hasbani et al., 2001; Tseng and Firestein, 2011). In our experiments, we activated glutamate receptors including NMDA receptors and blocked action potential firing with application of 100 µM L-Glu, 10 µM L-glycine, and 0.5 µM

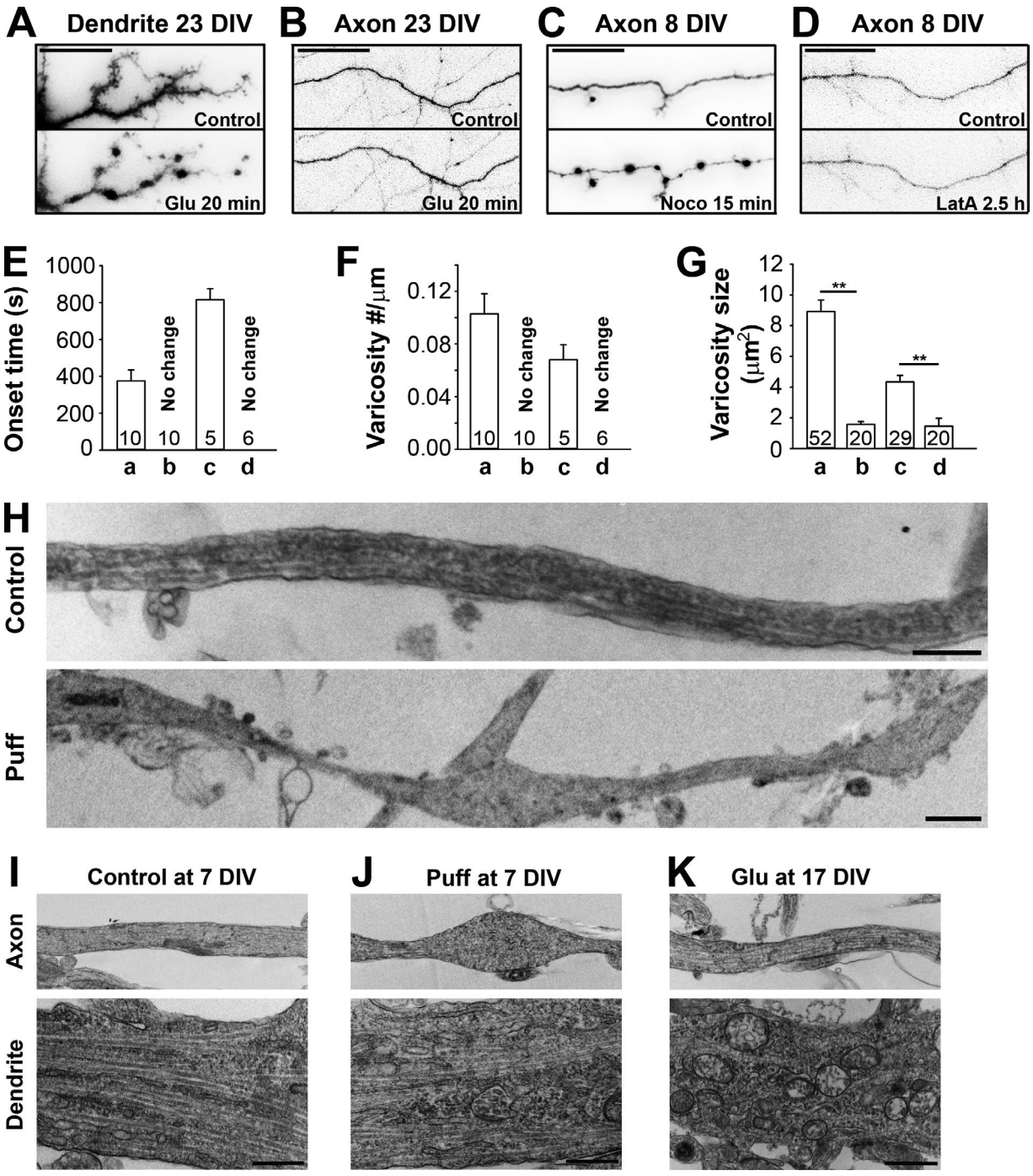

Figure 4. **MT disassembly in puffing-induced initiation of axonal varicosities.** (A and B) Stimulating NMDA receptors (100 μM L-glutamate, 10 μM L-glycine, and 0.5 μM TTX) for 20 min induced varicosities in dendrites (A) but not axons (B) in mature neurons (23 DIV). (C and D) Depolymerizing MTs by Noco (10 μg/ml for 15 min; C) but not actin filaments by LatA (2.5 μM for 2.5 h; D) induced varicosities in axons. (E–G) The onset time (E), density (F), and size (G) of induced varicosities along dendrites or axons under the conditions in A–D. In the drug treatment experiments, the onset time was defined as the time needed to form clear varicosities. Error bars indicate means ± SEM. Unpaired *t* test: **, $P < 0.05$. (H) Long axonal segments under control conditions (top) or developing multiple varicosities induced by puffing (bottom) were imaged by TEM. TEM experiments showed ultrastructural changes of axons (top) and dendrites (bottom) under control (7 DIV; I), puffing (7 DIV; J), and Glu treatment (17 DIV; K) conditions. Bars: (A–D) 25 μm; (H–K) 1 μm.

tetrodotoxin (TTX; a Na^+ channel blocker to suppress action potential firing). After ~20 min, varicosities were slowly induced along dendrites but not axons (Fig. 4, A and B; and Video 5). This effect is completely opposite to that of puffing (Fig. 1 F and Video 2). Therefore, axons and dendrites appear to form varicosities in response to mechanical stress (a physical stimulus) and Glu excitotoxicity (a chemical stimulus), respectively.

To determine whether actin or MT cytoskeleton is involved in axonal varicosity initiation, we treated neurons with 10 μg/ml nocodazole (Noco; depolymerizing MT filaments) or 2.5 μM latrunculin A (LatA; depolymerizing actin filaments). Noco but not LatA treatment induced axonal varicosities (Fig. 4, C–G). To visualize ultrastructural changes of axons and dendrites induced by puffing and Glu treatments, we performed

transmission EM (TEM). In 7-DIV control axons, MT tracts were clearly observed, whereas MT tracts were disrupted in the varicosities of the axons that received puffing (Fig. 4 H). Puffing-induced axonal varicosities displayed interesting heterogeneity: ∼50% of them with a few MTs remaining, ∼30% without any visible MT, and ∼20% with extensive vesicular structures. Although axonal varicosities formed, dendritic morphology was not altered by puffing (Fig. 4, I and J). In 17-DIV neurons, Glu treatment altered dendritic but not axonal structure, and dendrites became irregular in shape and contained many vesicle-shaped structures (Fig. 4 K). Therefore, the TEM results are consistent with the results of fluorescence imaging, showing that MT disassembly plays a key role in axonal varicosity initiation. MT disassembly can be induced by intraaxonal Ca^{2+} elevation. In fact, it was reported that Ca^{2+} directly binds to the C terminus of tubulin to destabilize MT filaments (Serrano et al., 1986; Lefèvre et al., 2011).

Persistent Ca^{2+} increase in puffing-induced axonal varicosities revealed by Ca^{2+} imaging

To determine whether puffing can indeed stimulate Ca^{2+} levels during axonal varicosity formation, we performed live-cell Ca^{2+} imaging on neuronal processes under control and puffing conditions. Cultured hippocampal neurons at 7 DIV were loaded with Fluo-4 AM, a Ca^{2+} indicator with increased fluorescence intensity and no shift in wavelength upon Ca^{2+} binding. Under the control condition without puffing, spontaneous Ca^{2+} transients were quite rare. The highest fluorescence intensity was observed in the soma and proximal dendrites, whereas the intensities in axons varied in a larger range, with some barely detectable. Under the same puffing condition that reliably induced axonal varicosity formation (Fig. 1), Fluo-4 AM fluorescence increased and sustained within axonal varicosities but not in intervaricosity axonal regions around the same time when axonal varicosities started to form (Fig. 5, A–E; and Video 6). In sharp contrast, under the same puffing condition, some transient increases of Ca^{2+} levels were observed in the entire dendrite in ∼30–50% of the neurons we examined (Fig. 5, F–J; and Video 7). Therefore, the spatial and temporal patterns of Ca^{2+} signaling were quite different in axons and dendrites in the puffing assay. The relatively persistent increase of Ca^{2+} levels in axonal spots where varicosities form may be more effective in causing MT disassembly. In vivo, however, the direct effect of Ca^{2+} on MT disassembly can be regulated by several factors, including MT-binding proteins.

MT-binding protein STOP plays an important role in axonal varicosity formation

To determine how stabilizing MTs may regulate axonal varicosity initiation induced by mechanical stress, we examined the effects of changing expression levels of three representative MT-binding proteins. MT filaments are polymeric cylinders composed of α/β tubulin dimers. Because of the head-to-tail arrangement of the dimers, MTs are intrinsically polarized. The plus end, where β tubulin is exposed, is the fast-growing end in vitro and the only end that grows in vivo. Several plus end–tracking proteins including EB1 specifically track the rapidly growing MT plus end, forming cometlike accumulations there. EB1 is a conserved small dimeric protein present in distal axons and plays a key role in regulating MT dynamics and MT-based protein targeting (Gu et al., 2006; Akhmanova and Steinmetz, 2008). It is important to note that EB1 proteins do not move along MTs processively but exchange rapidly at MT plus ends by recognizing some specific structural features of the growing end. Overexpressed EB1 can stabilize MT filaments by promoting MT elongation and bundling (Bu and Su, 2001; Ligon et al., 2003) and is often used to reveal MT dynamics (Zheng et al., 2008). In our experiments, expressing EB1-YFP in hippocampal axons did not change puffing-induced varicosity initiation (Fig. 6, A and D).

However, MT-associated protein 2 (MAP2) is mainly enriched in dendrites and binds to both tubulin and actin. MAP2 induces MT bundling likely via cross-linking MTs by MAP2 dimerization (Sánchez et al., 2000; Koleske, 2013). Is it possible that the high expression level of MAP2 in dendrites renders their resistance to puffing-induced varicosity formation? We overexpressed YFP-MAP2 into hippocampal neurons. Although it was mainly enriched in dendrites, there was a significant amount of YFP-MAP2 present in axons. Significantly higher levels of YFP-MAP2 did not alter puffing-induced varicosity formation in axons either (Fig. 6, B and D).

Another MT-binding protein, STOP (NSTOP is the splice variant of adult form), was initially isolated as a calmodulin-binding protein associated with purified rat brain cold-stable MTs (Margolis et al., 1986; Bosc et al., 1996). STOP has intrinsic MT cold stabilizing activity in vitro, which is inhibited by Ca^{2+}-bound calmodulin (Pirollet et al., 1992). STOP proteins are expressed in both developing and adult brains, localized in axons, and are likely responsible for a high degree of MT stabilization observed in neuronal cells (Guillaud et al., 1998; Couégnas et al., 2007; Richard et al., 2009). Reduced STOP expression in mice leads to synaptic deficits as well as behavioral and cognitive disorders (Andrieux et al., 2002; Eastwood et al., 2007; Fournet et al., 2012). In sharp contrast with EB1-YFP and YFP-MAP2, hippocampal axons expressing NSTOP-GFP became markedly resistant to puffing-induced varicosity formation (Fig. 6, C and D). Therefore, STOP that is regulated by Ca^{2+}/calmodulin may play a key role together with TRPV4 in shaping the mechanics-mediated response of hippocampal neurons.

To reveal the temporal and spatial expression of STOP in neurons, we used both anatomical and biochemical techniques. During maturation of the CNS, the total protein levels markedly increased for STOP but not for TRPV4, as revealed by Western blotting (Fig. 6 E). Next, we examined the expression and localization patterns of STOP in the mouse brain at different developmental stages and found that they were consistent with the immunoblotting results. Immunostaining of adult brain sections showed that STOP was present along axonal fibers in the hippocampus, whereas the level of TRPV4 was higher in the soma and proximal processes (Fig. 6 F). Therefore, the differential expression and targeting patterns of STOP and TRPV4 appear consistent with our finding that younger and distal axons are more likely to form varicosities under mechanical stress. Neuronal expression of STOP was further confirmed in cultured rat hippocampal neurons. STOP was expressed in hippocampal neurons and relatively concentrated in the soma as well as in proximal dendrites and axons (Fig. 6, G and H; and Fig. S5). Because proximal axons, including the axon initial segment (AIS), were relatively resistant to puffing-induced varicosity formation compared with distal axons (Figs. 1 C and S2), endogenous STOP appears to be enriched in the neuronal compartments that are relatively resistant to puffing.

To verify STOP's role in axonal varicosity initiation, we examined the effect of knocking down STOP using siRNA. The

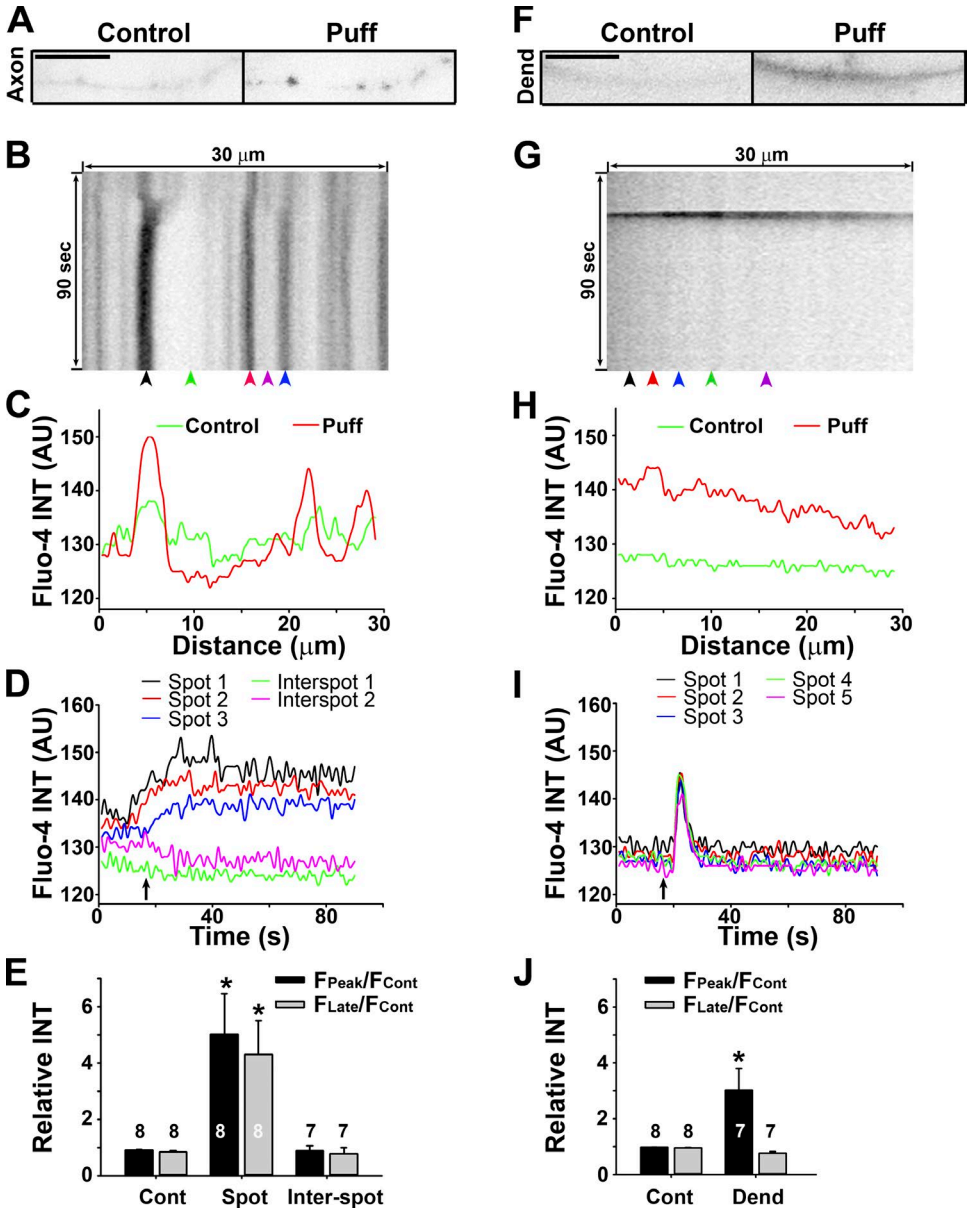

Figure 5. **Sustained Ca^{2+} increase in axonal varicosities induced by mechanical stress.** (A) An axonal segment before (0 s; control) and after (50 s; Puff) puffing. Signals are inverted. (B) Kymograph of Fluo-4 fluorescence along the axonal segment in A. (C) Fluorescence profiles along the axonal segment at two time points in A. (D) Fluorescence intensities (INT) over time at five different locations indicated by arrowheads in B. (E) Summary of intensity changes of Fluo-4 fluorescence without (Cont) and with (Spot, in a varicosity; Inter-spot, between varicosities) puffing. (F) A dendrite before (0 s) and after (25 s) puffing. Bars, 10 µm. (F) Kymograph of Fluo-4 fluorescence along the dendrite in F. (H) Fluorescence profiles along the dendrite at two time points in F. (I) Fluorescence intensities over time at five different locations indicated by arrowheads in G. (J) Summary of intensity changes of Fluo-4 fluorescence without and with (Dend) puffing. F_{cont}, fluorescence intensity before puffing; F_{Peak}, the maximal fluorescence intensity reached during puffing; F_{Late}, fluorescence intensity at 80 s; arrows, the puffing onset. Background was not subtracted in C, D, H, or I. Background was subtracted in E and J. Error bars indicate means ± SEM. A one-way ANOVA followed by Dunnett's test was used in E and an unpaired *t* test was used in J. *, $P < 0.05$.

siRNA probe was previously published and used to successfully knock down endogenous STOP in cultured subicular neurons in mice (Deloulme et al., 2015). In control mouse hippocampal neurons at 10 DIV, endogenous STOP was concentrated in the proximal axon and tapered off near the distal end of the middle axon (Fig. 7, A and B). In the neurons transfected with STOP siRNA, endogenous STOP was largely absent, indicating successful knockdown (Fig. 7, C and D). When being puffed, the middle axons of the neurons (10 DIV) transfected with STOP siRNA developed more varicosities much faster with larger varicosity size compared with those of the control neurons (Fig. 7, E and F). This effect was reversed by coexpression of NSTOP construct (rat), in which the neurons were cotransfected with NSTOP-GFP and mouse STOP siRNA (Fig. 7, G and H). Collectively, our results have indicated that STOP plays an important role in puffing-induced varicosity formation in axons, most likely through mediating Ca^{2+}-dependent regulation of MT stability.

MT plus end tracking and axonal transport of mitochondria and synaptic proteins pause in axonal varicosity initiation

In axons, most MTs are oriented with the plus end toward the axonal growth cone and with the minus end toward the soma.

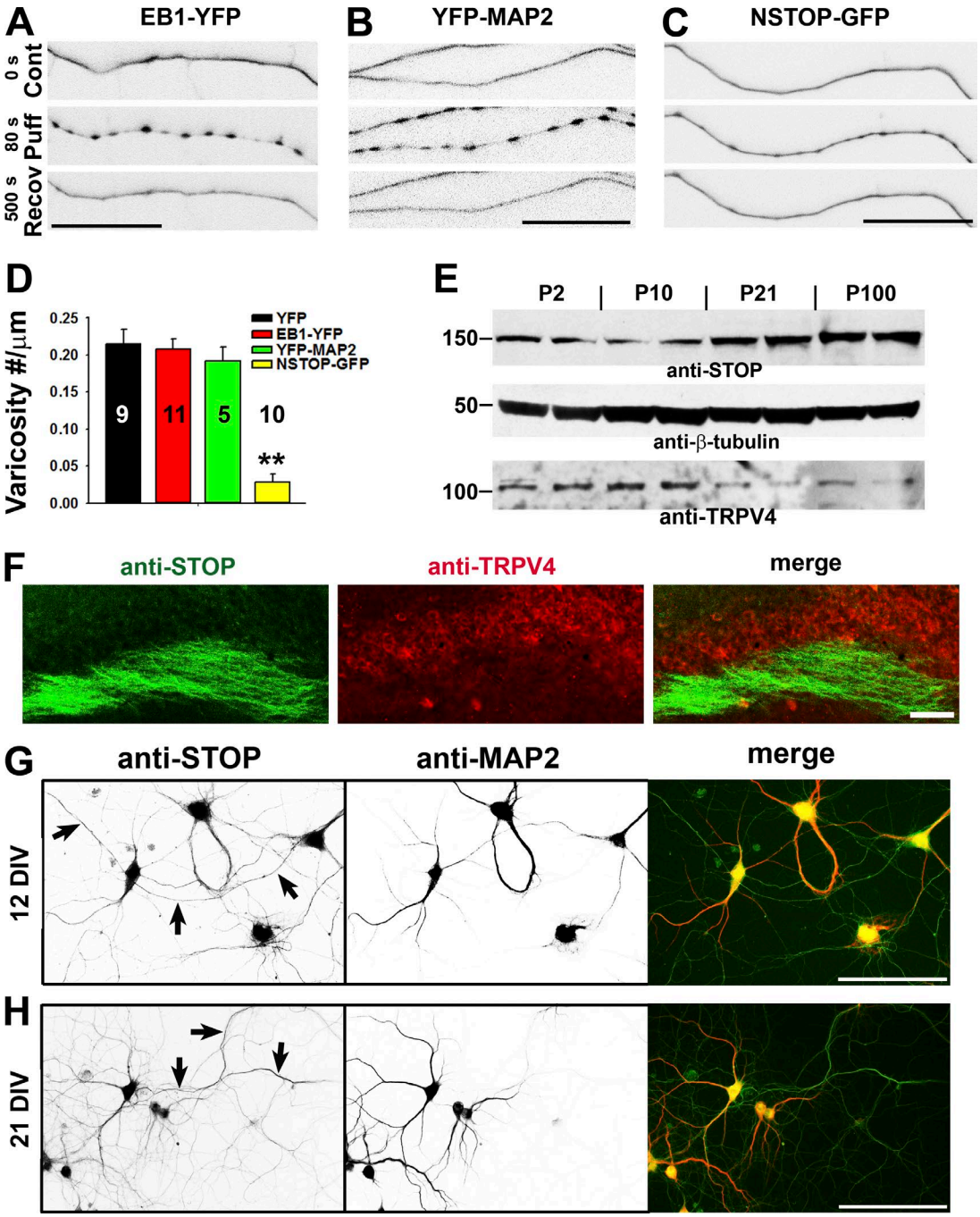

Figure 6. **The level of MT-binding protein NSTOP correlates with the resistance of puffing-induced varicosity formation.** (A and B) Axons expressing different MT-binding proteins were puffed, and expressing EB1-YFP (A) or YFP-MAP2 (B) in axons did not change puffing-induced varicosity formation. (C) The axon expressing NSTOP-GFP became more resistant to puffing. (D) Summary of the effects of three MT-binding proteins on axonal varicosity formation. Error bars indicate means ± SEM. One-way ANOVA followed by Dunnett's test: **, $P < 0.01$. (E) Expression levels of STOP and TRPV4 in the brain during development. Western blotting for STOP and TRPV4 from mouse brain lysate was performed, and β-tubulin was used as a control. Molecular masses are indicated in kilodaltons. (F) Costaining for endogenous STOP (green) and TRPV4 (red) in the hippocampal slice of an adult mouse. (G and H) Costaining for endogenous STOP (green in merged) and MAP2 (red in merged) was performed in cultured hippocampal neurons at 12 DIV (G) and 21 DIV (H). Arrows indicate MAP2-negative axons containing anti-STOP staining signals. Bars: (A–C) 25 µm; (F–H) 100 µm.

How does axonal varicosity formation affect MT dynamics, especially the plus end dynamics? Could MT orientation be reversed during MT reassembly after varicosity formation? Using live-cell imaging of EB1-YFP–expressing axons of cultured hippocampal neurons, we visualized the anterograde and retrograde movements of EB1-YFP before, during, and after puffing. We found that MT plus-end tracking paused during puffing-induced varicosity formation and slowly recovered afterward, consistent with MT disassembly induced by puffing and MT reassembly during recovery (Fig. 8 A). Importantly, the orientation of MT plus end tracking did not change during MT reassembly after puffing. Interestingly, the tracking velocity, distance, and frequency did reduce after puffing compared with those before puffing (Fig. 8, D–F). This result suggests

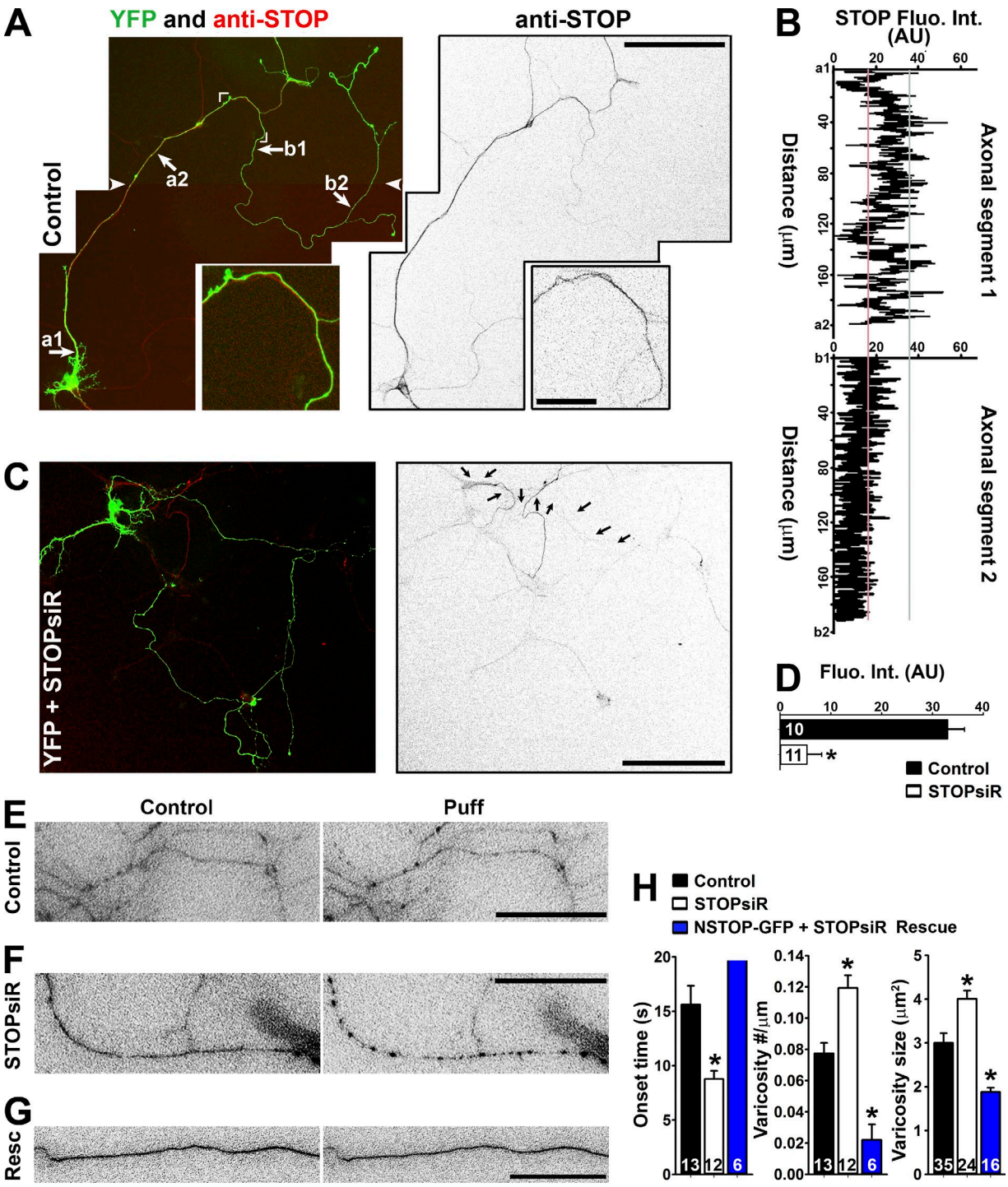

Figure 7. **Axonal distribution of STOP and its knockdown on varicosity formation.** (A) Endogenous STOP (red in merged image on the left; inverted grayscale on the right) expression from neurons at 10 DIV. Cornered area, enlarged (2.5-fold) bottom panels. White arrowheads show the montage line of two overlapping images. (B) STOP fluorescence intensities along two labeled axonal segments in A. (C) Significant reduction of STOP in the neuron transfected with STOP siRNA (siR). Arrows indicate the axon of the transfected neuron. (D) Summary of the effect of STOP siRNA knockdown along middle axons. Mean fluorescence intensity was measured from a segment of middle axons from control (black bar) and STOPsiR (open bar) neurons. Unpaired *t* test: *, $P < 0.05$. (E) Middle axons transfected with YFP and control siRNA were puffed. YFP signals were inverted. (F) A middle axon transfected with YFP and STOP siRNA was puffed. (G) A middle axon transfected with NSTOP-GFP (rat) and STOP siRNA was puffed. Resc, Rescue. (H) Summary of the puffing results for the effects of STOP siRNA on onset (left), varicosity number (middle), and size (right). Mouse hippocampal neurons were cultured from mouse pups at P0–P2. Error bars indicate means ± SEM. One-way ANOVA followed by Dunnett's test: *, $P < 0.05$. Bars: (A [main images] and C) 100 μm; (A, inset) 20 μm; (E–G) 15 μm.

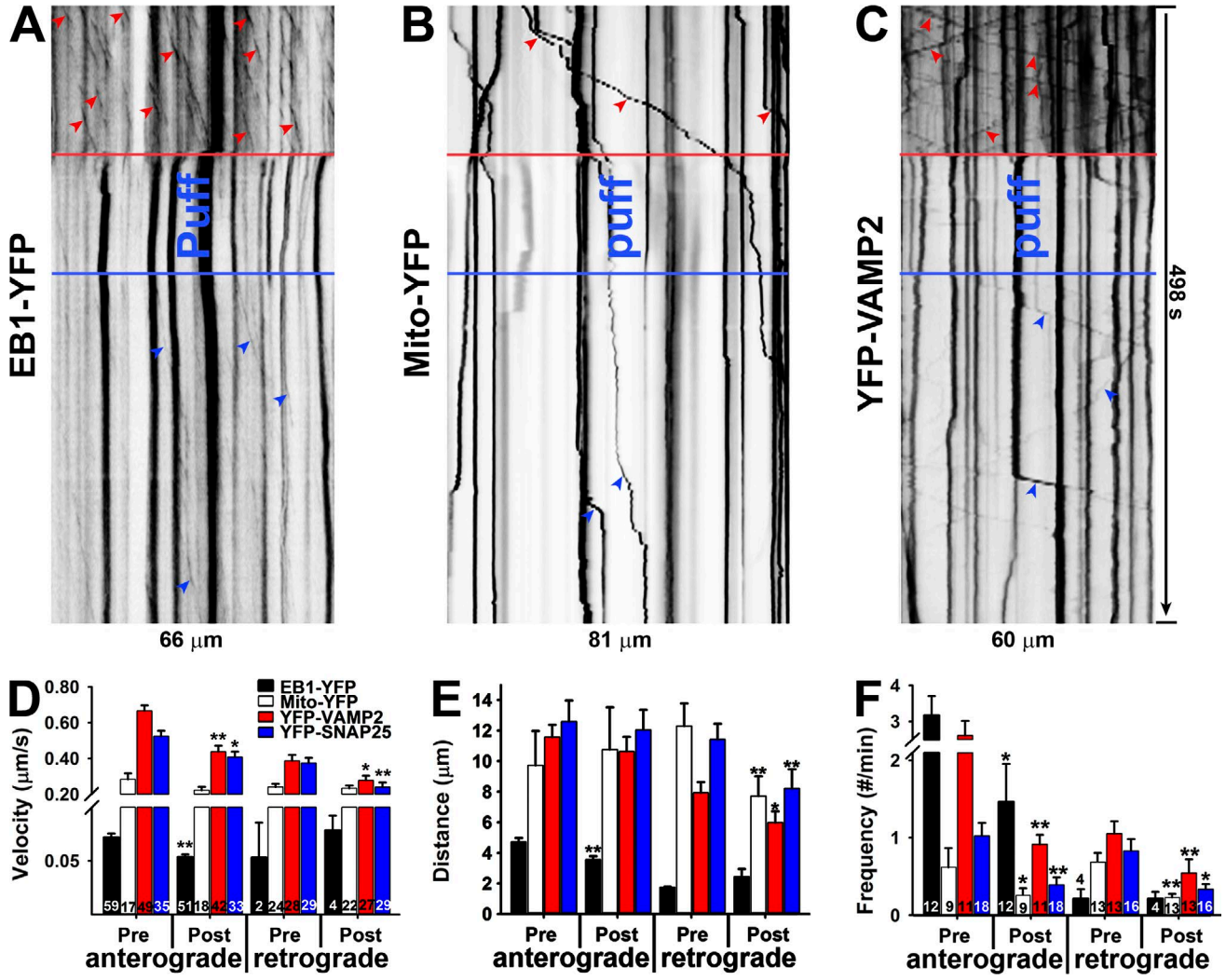

Figure 8. **Mechanics-induced axonal varicosities are accompanied with transiently halted MT dynamics and axonal transport.** (A) Kymograph of EB1-YFP plus end tracking before, during, and after puffing along an axonal segment. (B) Kymograph of Mito-YFP transport before, during, and after puffing along an axonal segment. (C) Kymograph of YFP-VAMP2 transport before, during, and after puffing along an axonal segment. Red arrowheads show movements before puffing, and blue arrowheads show movements after puffing. (D–F) Effects of puffing on moving velocity (D), distance (E), and frequency (F) of EB1-YFP plus end tracking, mitochondria transport, and presynaptic protein transport in anterograde and retrograde directions. Error bars indicate means ± SEM. Unpaired *t* test between pre- and post-puffing: *, $P < 0.05$; **, $P < 0.01$.

that MT plus end dynamics, although not reversed, are altered at least transiently during axonal varicosity formation induced by mechanical stress.

Crucial for axonal functions is proper MT-based axonal transport of organelles and proteins, including mitochondria and presynaptic proteins. Their transport in both anterograde and retrograde directions was observed (Kang et al., 2008; Wang and Schwarz, 2009; Barry et al., 2014). We wondered how fast puffing-induced MT disassembly affects their axonal transport and in which direction the transport may be disrupted. We also wondered whether newly reassembled MTs can immediately support axonal transport in both directions. Mito-YFP contains a mitochondria-targeting motif and is specifically localized in mitochondria. When expressed in hippocampal neurons, both anterograde and retrograde movements were observed, paused during puffing-induced varicosity formation, and recovered after puffing was stopped (Fig. 8, B and D–F). We further examined two synaptic proteins, VAMP2 (a v-SNARE) and synaptosomal-associated protein 25 (SNAP-25; a t-SNARE). YFP-VAMP2 and YFP-SNAP25 were expressed in hippocampal neurons. Both moved along axons in anterograde and retrograde directions, paused during puffing, and resumed movements after puffing (Fig. 8, C–F). Collectively, axonal transport largely stopped during puffing-induced axonal varicosity formation, reflecting MT disassembly, and immediately resumed when puffing stopped, albeit with lower transport frequency in both directions. There were some reductions in transport velocity and distance. Moreover, during puffing, MT disassembly disrupted general axonal transport in both anterograde and retrograde directions, which likely led to an accumulation of axonal contents and hence the formation of varicosities.

A new form of rapid axon–soma communication during axonal varicosity formation

Axotomy of dorsal root ganglion neurons causes the back-propagation of Ca^{2+} waves at the speed of 10 μm/s, which invade the soma and initiate injury-related transcription programs (Cho et

al., 2013). Is the neuronal soma able to detect axonal varicosity formation induced by mechanical stress? If yes, how fast can the soma detect it? To determine the potential electrical signaling during axonal varicosity formation induced by puffing, we simultaneously performed whole-cell patch-clamp recording from the neuronal soma along with time-lapse imaging of axonal segments that were ∼300 µm away from the soma and received puffing (Fig. 9 A). Remarkably, puffing could induce action potentials antidromically propagating to the soma during varicosity initiation in both young and old neurons (Fig. 9, B and C). Although axonal varicosities were reliably induced, back-propagating action potentials were only recorded from ∼30% of neurons. Their onset time also varied greatly, from 2–100 s (Fig. 9 D), suggesting that puffing-induced varicosity initiation can be rapidly detected by the soma through antidromic action potential propagation in some neurons. The variation may result from diverse availability and regulation of voltage-gated sodium (Nav) channels in different axonal branches.

Previous studies suggest that Nav channel activity can be regulated by mechanical stress (Morris and Juranka, 2007; Beyder et al., 2010). In hippocampal neurons cultured at 7 DIV, endogenous Nav channels are mainly concentrated at the AIS (Barry et al., 2014). To examine a potential role of Nav channel in puffing-induced varicosity formation, we first transfected the hippocampal neurons with Nav1.2-GFP cDNA construct. Nav1.2 is the major isoform expressed in young hippocampal neurons. Nav1.2-GFP was mainly concentrated at the AIS in the proximal axon, where no varicosity was induced by puffing (Fig. S6 A). Our previous study showed that knocking down endogenous Ankyrin-G (AnKG) eliminated endogenous Nav channels in axons (Barry et al., 2014). Neither overexpressing AnkG-GFP nor knocking down AnkG with shRNA allowed the AIS to form varicosities when being puffed (Fig. S6, B and C). Thus, Nav channels and AnkG-clustered AIS components are unlikely to be involved in puffing-induced axonal varicosities. Collectively, our study shows that axonal varicosity initiation is likely accompanied by a receptor potential via TPRV4 activation, which can trigger action potential (via Nav channel activation) antidromic propagation, a much faster axon–soma communication compared with Ca^{2+} waves and retrograde transport.

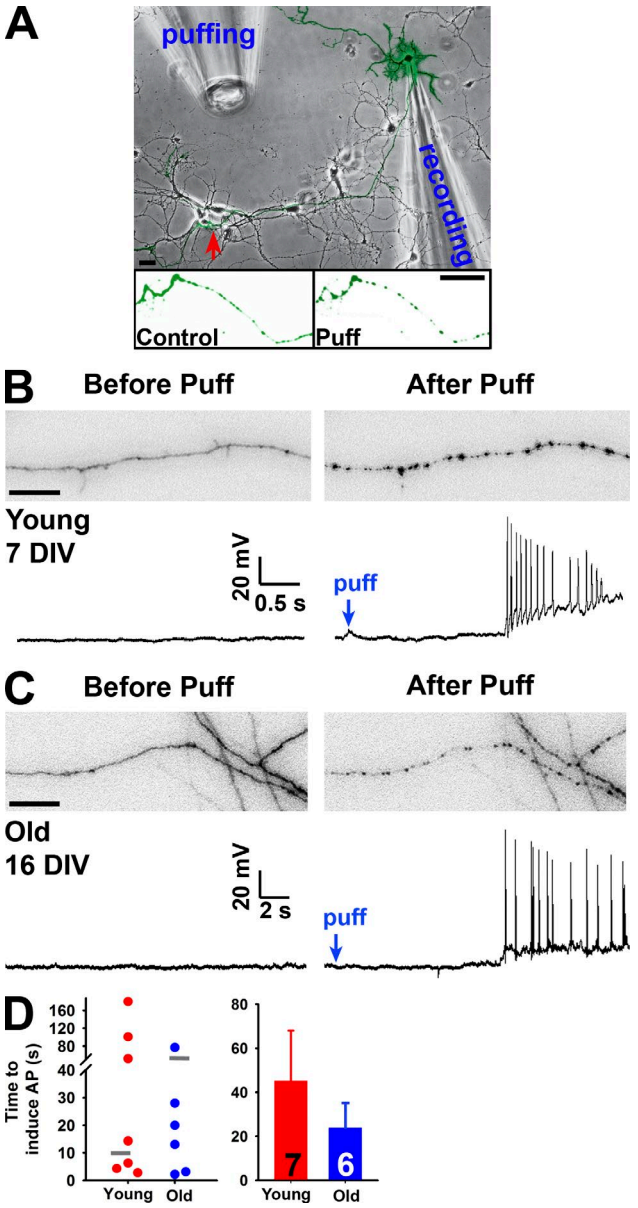

Figure 9. **Axonal varicosity initiation can induce antidromic propagation of action potentials.** (A) Experimental diagram of recording back-propagating action potentials initiated by puffing. The YFP-expressing neuron over the transmitted-light background was recorded by a patch pipette at the soma. Its axons received mechanical stimuli provided by the puffing pipette. The red arrow indicates the area containing YFP-positive axons shown before (Control; left) and after (Puff; right) puffing. (B) Simultaneous imaging of an axonal segment (top) and whole-cell current-clamp recording (bottom) of a young neuron (7 DIV) before (left) and after (right) puffing. (C) Simultaneous imaging of an axonal segment (top) and whole-cell current-clamp recording (bottom) of a more mature neuron (16 DIV) before (left) and after (right) puffing. Bars: (A) 30 µm; (B and C) 20 µm. (D) Summary of the time to induce action potentials for all neurons (left) and means ± SEM (right). Gray short lines in the left panel indicated the mean time for axonal varicosity initiation. AP, action potential. Error bars indicate means ± SEM.

Discussion

Our study has demonstrated rapid, reversible, and polarized varicosity initiation in central neuron mechanosensation. This process depends on the strength and duration of mechanical stress, neuron age, and importantly, subcellular compartment. Based on our results, we propose the following mechanistic model that micromechanical stress activates TRPV4 in axonal membranes, leading to Ca^{2+} influx into the axon. Subsequently, increased Ca^{2+}-bound calmodulin levels in the axon compete with STOP for MTs, which destabilizes MTs and thus disrupts normal axonal transport, further leading to aberrant accumulation of axonal cargos and formation of axonal varicosities (Fig. 10, A and B). Our findings suggest a potentially new pathogenic mechanism underlying repeated subconcussive brain injury. For a glutamatergic CNS neuron, mechanical stresses are likely first sensed by its axon but not dendrites and then broken axonal segments release glutamate to damage dendrites and soma via excitotoxicity (Fig. 10, C–E). Furthermore, our results have revealed a novel and rapid axon–soma communication upon varicosity initiation mediated by back-propagating action potentials.

The puffing pressure (0.25 ± 0.06 nN/µm^2) onto the neurons in our experimental setting is physiologically or pathologically relevant. It does fall within the range of what previous

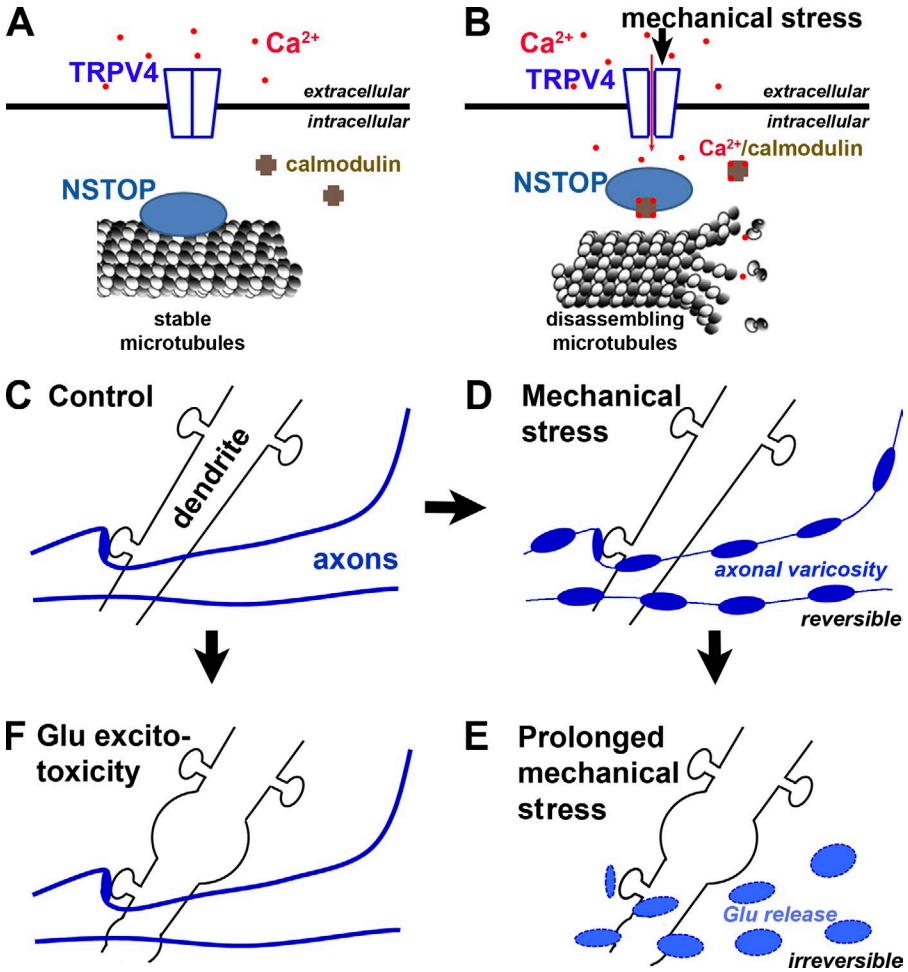

Figure 10. **A new model of polarized initiation of neuronal varicosities induced by mechanical stress.** (A) Diagram of signaling molecules on both sides of axonal membrane under control condition. (B) Mechanical stress induces a signaling cascade across the axonal membrane to induce axonal varicosity formation. (C–E) A new model diagram of sequential axonal and dendritic swelling under pathological mechanical stress. (C) Dendrites, dendritic spines, and axons under normal conditions. (D) Under mechanical stress, axonal varicosities start to form while dendrites and dendritic spines remain unchanged. (E) Under prolonged or pathological mechanical stresses, axonal varicosities become irreversible and are eventually broken to release the neurotransmitter glutamate, which can overstimulate its receptors on dendrites to induce swelling and hence neuronal death. (F) Prolonged stimulation of Glu (particularly NMDA) receptors causes swelling in dendrites but not in axons.

investigators used in in vitro and in vivo studies. Using scanning force microscopy, an early study reported that the applied stress (0.27 ± 0.04 nN/μm^2) altered exploratory behaviors of the leading edge of neurite processes in vitro in a neuronal cell line (Franze et al., 2009). Currently, it is still not feasible to accurately measure micromechanical pressures within a living brain. Limited progress was made for measuring mechanical stress in vivo. Using fluorescent cell-sized oil microdroplets with defined mechanical properties, a recent study estimated that the maximal anisotropic stress generated by mesenchymal cells in living embryos at the stage E11 was $\sim 1.6 \pm 0.8$ nN/μm^2 (Campàs et al., 2014). Interestingly, the value of puffing pressure in our setting is similar to that of the elastic modulus of hippocampal neurons, which was measured with scanning force microscopy, bulk rheology, and optically induced deformation to reflect viscoelastic characteristics of pyramidal neurons (Lu et al., 2006; Elkin et al., 2007). Besides the variation among different cell types, the stiffness of soma and neurites can differ (Grevesse et al., 2015). If the external pressure equals the elastic modulus of the material with an ideal linear elastic property and an infinite yield strength, a large deformation with 100% strain would be achieved. However, because cells are viscoelastic and stress-responsive materials, the viscosity, loading rate, and mechanical adaptation in addition to compressive pressure are required to be considered in calculating the deformation. Nonetheless, the pressure of such value should induce significant deformation to neurons and subsequently cause cytoskeleton remodeling, mechanical adaptation, or even damage.

In our experimental setting, the mechanical stress mainly consists of out-of-plane compression and shearing. There was no gross movement of neuronal processes as a result of good attachment to coverslips. This is different from other experimental settings mainly involving bending and in-plane stretching (or tension) such as, for instance, deflection of axonal bundles like moving strings (Chung et al., 2005; Staal et al., 2007) or stretching axons growing on micropatterned channels or stretchable membranes (Hemphill et al., 2011; Tang-Schomer et al., 2012). Consistent with our results, all of these can also induce axonal varicosities. However, in sharp contrast, axonal varicosity formation in these settings takes much longer (from 10 min to several hours; Staal et al., 2007; Hemphill et al., 2011; Tang-Schomer et al., 2012) to develop and appears irreversible. Therefore, our assay system is very different from those existing in vitro systems and provides novel insights into central neuron mechanosensation.

Under our experimental condition, we show two unexpected features of axonal varicosity formation induced by mechanical stress, rapidness, and reversibility. The initial appearance of axonal varicosities under our condition was <5 s for young neurons (Fig. 1), which was not reported before. The onset time increased when the neurons become more mature, likely in part because the expression and localization patterns of the MS channels TRPV4 and STOP change in mature neurons (Figs. 3, 6, S4, and S5). It is important to note that the moderate reduction of endogenous TRPV4 level in mature axons is not complete elimination, and thus our results are still relevant

to the mature brain. Moreover, TRPV4 level change, in sharp contrast with the marked increase of STOP proteins, is likely uneven in different neurons of the mature brain, consistent with the uneven injury of a subset of axons in mTBI. Furthermore, myelination increases with maturation of the CNS. Myelin membranes may effectively insulate older axons from ionic influx and hence prevent axonal varicosity formation under mild micromechanical stress (Fig. 1 A), representing a potentially novel role of axonal myelination. Collectively, it will be interesting to further determine whether these factors can indeed make a mature brain more resistant to an mTBI or concussive brain injury than a young brain in future studies.

Dendritic varicosities are likely induced through a very different pathway. In comparison, the induction of dendritic varicosities by a pathological level of glutamate took ∼20 min (Fig. 4). This is ∼100-fold slower than puffing-induced varicosity formation in axons. Thus, these two events appear to have different underlying mechanisms. Furthermore, histochemical studies using mouse models of mTBI revealed the changes in the brain, including axonal and dendritic varicosities, only over a much longer period, from a few hours to several days (Reeves et al., 2005; Gao et al., 2011). Our study suggests that formation of axonal and dendritic varicosities may take place at different time courses because of different underlying mechanisms.

Axonal varicosities induced in vivo and in vitro in various disease or injury models are usually thought to be irreversible as a sign of axon degeneration. Unexpectedly, our study shows that the transient formation of axonal varicosities induced by mechanical stress is actually reversible, although it takes a much longer time to recover than that to initiate (Fig. 1 G). The reversibility may be caused by the micromechanical pressure we applied, which likely resembles the situation in a subconcussion, and which can recover. However, repeated subconcussions can still lead to accumulative permanent brain injury, just like what we found for hippocampal axons under repeated short pulses of puffing (Fig. 1 H). The reversibility of puffing-induced axonal varicosities in this study is consistent with the observation that some axonal swellings can be spontaneously reversed in a few hours in a mouse model of multiple sclerosis (Nikić et al., 2011). However, it is not known whether micromechanical stress plays a role there because of potential tissue swelling induced by inflammation. Furthermore, the reversibility of varicosity formation allows it to be involved in normal neural development or even in the adult brain as a novel form of neural plasticity.

Our previous study using a repetitive closed-skull impact model (Shitaka et al., 2011) confirmed that mild mechanical stress can indeed induce axonal varicosities in vivo (Fig. 2). There are several other animal models for studying repetitive mTBI (Kanayama et al., 1996; Laurer et al., 2001; DeFord et al., 2002). In general, the pathological features of the injury appeared relatively subtle in comparison with the extent of the behavioral deficits (Shitaka et al., 2011). This might be because of the sensitivity of histological tools and potential recovery of structural alterations. In our study, we fixed the mice immediately after the second impact instead of 6 d later in the prior study (Shitaka et al., 2011). This allowed us to better capture the initiation of axonal varicosities (Fig. 2), whereas axonal varicosities with staining of amyloid precursor protein (APP) were rare 6 d later (Shitaka et al., 2011), which might result from recovery. Alternatively, APP staining likely represents degenerating axons but does not exist in transient and reversible formation of axonal varicosities. In addition, we used Thy1-YFP transgenic mice in our study, which allow better detection of axons and axonal varicosities. Multifocal axonal injury and other changes in different brain regions were previously detected in this model (Shitaka et al., 2011). Consistent with these findings, we did observe axonal varicosities in the multifocal fashion in our study, which supports our results from cultured neurons. It is important to note that a more comprehensive study would include examination of the effects on neurons by altering the strength, number, and interval of mechanical impacts. Perhaps the most informative strategy is to perform in vivo imaging of neuronal morphology before, during, and after mechanical impact. Unfortunately, this technique currently is not yet available. Nonetheless, our in vivo results not only show axonal varicosity formation but also raise several interesting questions for future studies.

The closed-skull impact model has been established for studying mTBI (Shitaka et al., 2011). Our in vitro puffing model mimics many aspects of mTBI as well in terms of the moderate strength, compression and shearing stresses, varicosity formation, and recovery that we have discussed. On the other hand, during mTBI, the contact between an object and the skull of the head is usually very short, shorter than the time needed for puffing-induced varicosity formation in axons. However, it is important to note that there is a spring-dashpot system between the impact point at the skull and the neurons because of the presence of elastic tissues and the cerebrospinal fluid in between. The system affects the stress magnitude and the moment of peak stress. In particular, it may take longer to reach the peak stress value, and the force may last longer than that for the initiate impact for various neurons in the brain to be compressed, torn, or stretched, causing membrane deformation that activates MS ion channels. Furthermore, varicosity formation, which is the readout of our puffing assay, involves multiple steps after the initial mechanical loading and takes more time to develop, as illustrated in our summary diagram (Fig. 10, A and B). Therefore, our findings with the puffing system are relevant to concussion or mTBI.

Our study has provided several lines of evidence showing that TRPV4 functions as the major MS ion channel in mechanical stress–induced varicosity formation in the axons of hippocampal neurons: (a) TRPV4 was permeable to Ca^{2+} and, to a lesser extent, Na^{+} (∼1:6 ratio), which is consistent with the effects of removing the two cations in axonal varicosity initiation (Fig. S3, A–D); (b) TRPV4 agonist perfusion induced axonal varicosity formation (Fig. S3, E–G); (c) two TRPV4 antagonists blocked puffing-induced varicosity formation (Fig. S3, E–G); (d) TRPV4 expressed in HEK293 cells was activated by puffing (Fig. 3, A–C); and (e) TRPV4 was detected in the axons of hippocampal neurons, consistent with a previous study (Shibasaki et al., 2007), and its knockdown by shRNA reduced puffing-induced axonal varicosity initiation (Figs. 3 and S4). Collectively, these data indicate a key role of TRPV4. However, at this time, we cannot completely rule out the potential role of other unidentified and Ca^{2+}-permeable MS ion channels in this process. Therefore, it will be interesting to determine how different expression of potential MS channels in various CNS neurons may be responsible for neurons' distinct sensitivity to various mechanical stresses in future studies.

Neuronal morphological and functional polarity has been extensively investigated. Our study has demonstrated for the first time that micromechanical stress and excitotoxicity preferentially affect axons and dendrites, respectively (Figs. 1 and

4). Dendritic varicosities were induced by glutamate (plus glycine and TTX) in ∼20 min (Fig. 4), consistent with the time course of previous studies using sublethal NMDA exposure (Hasbani et al., 2001; Tseng and Firestein, 2011). A previous study showed that prolonged activation of NMDA receptors led to MT fragmentation, in which two postsynaptic proteins, PDS-95 and Cypin, played regulatory roles (Tseng and Firestein, 2011). Under our treatment condition, we cannot rule out the potential role of other types of glutamate receptors. Because of dendritic localization of NMDA receptors (and other glutamate receptors) and downstream signaling, excitotoxicity may initiate only in dendrites, but not axons. However, degeneration of neuronal dendrites and soma eventually led to axon degeneration. In sharp contrast, micromechanical stress preferentially affected axons in which MS channel TRPV4 is relatively enriched and the MT-stabilizing effect of STOP can be reversed (Figs. 3 and 6). For both excitotoxicity and mechanical stress–induced varicosities, Ca^{2+} influx and subsequent MT disassembly play critical roles. Under the puffing condition, our live-cell imaging experiments show that the spatial and temporal patterns of Ca^{2+} signaling are different in axons and dendrites. Ca^{2+} increases accompanied axonal varicosity formation and were relatively more persistent, whereas there were only transient Ca^{2+} increases (<20 s) in some dendrites (Fig. 5). This may result from a strong Ca^{2+} sequestration mechanism in dendrites, which may only be overpowered by excitotoxicity. Why does replacing external Na^+ with NMDG render axons some resistance to puffing-induced varicosity initiation? Na^+ influx can activate voltage-gated Ca^{2+} channels by depolarizing the axonal membrane and reverse Na^+/Ca^{2+} exchangers (Barsukova et al., 2012), leading to additional Ca^{2+} increase in axons. In the absence of external Ca^{2+}, Na^+ influx may indirectly lead to a minor Ca^{2+} increase via the release from internal Ca^{2+} stores (Barsukova et al., 2012). Therefore, external Na^+ may indirectly regulate intraaxonal Ca^{2+} levels, whereas Ca^{2+} plays a central role in puffing-induced varicosity initiation. Furthermore, a markedly larger volume in dendrites also requires significantly more Ca^{2+} cations to reach a higher free Ca^{2+} concentration and/or to depolarize the membrane. The same puffing pressure may induce less deformation in dendrites compared with axons, leading to less activated TRPV4 ion channels in dendrites. The TRPV4 protein levels on the neuronal surface are still not clear, and maybe are less on dendritic membranes. All of these factors contribute to the result that mechanical stress is less likely to induce varicosities in dendrites. More extensive studies using Ca^{2+} imaging in vivo and combined with imaging of MS channel activation and MT dynamics/stability are interesting research topics for future investigation.

The MT cytoskeleton plays a key role in the establishment and maintenance of neuronal polarity. MT dynamics and stability in neurons can be regulated through different mechanisms, including many different MT-binding proteins (Baas et al., 2016; van Beuningen and Hoogenraad, 2016). In our study, we have tested three MT-binding proteins, EB1, MAP2, and STOP, when overexpressed, which can stabilize MTs in very different ways. Our results show that EB1 and MAP2 are not likely involved in puffing-induced axonal varicosity initiation, whereas STOP likely plays an important role because overexpressing NSTOP-GFP inhibited this process (Fig. 6, A–D). Interestingly, endogenous STOP proteins were not evenly distributed along an axon, with the highest level in proximal axons and the lowest level in distal axons (Fig. 7, A and B). The high levels of STOP proteins in proximal axons as well as in soma and dendrites are consistent with the results that these regions are more resistant to puffing-induced varicosity formation (Fig. 1) and that the axons with overexpressed NSTOP-GFP are varicosity resistant (Fig. 6, C and D). However, the moderate level of STOP in middle and distal axons may allow it to reversibly regulate MT stability in response to different Ca^{2+}/calmodulin levels with the axon. To confirm its important role in this process, we performed siRNA knockdown of endogenous STOP and found that the middle axons from mouse hippocampal neurons transfected with STOP siRNA became significantly more sensitive to puffing, which was reversed or rescued when NSTOP-GFP (rat) was cotransfected (Fig. 7, C–H). It is important to note that this experiment was performed using mouse hippocampal neurons cultured from postnatal pups because the published STOP siRNA is mouse specific (Deloulme et al., 2015). Furthermore, these results indicate that not all axons are equally sensitive to micromechanical stress, consistent with the previous results from mTBI models (Reeves et al., 2005). Myelinated, aged, and proximal axons are relatively more resistant to mechanical stress (Figs. 1 and S2), likely resulting from less Ca^{2+} influx and more rigid MT filaments.

Interestingly, STOP was initially discovered by its function of stabilizing MT filaments at cold temperatures (Margolis et al., 1986; Bosc et al., 1996), whereas TRPV4 activity can be regulated by temperature changes (Christensen and Corey, 2007; Venkatachalam and Montell, 2007). Temperature is a physical factor. Therefore, our study leads to a novel model in which axons and dendrites of CNS neurons may be designed to selectively sense and respond to physical and chemical stimuli, respectively. In younger neurons, there are relatively higher TRPV4 and lower STOP levels compared with older neurons. The similar pattern exists for distal axons compared with proximal axons. Higher TRPV4 activity leads to more Ca^{2+} influx induced by mechanical stimuli, and lower STOP levels are more likely to cause Ca^{2+}-mediated MT disassembly, which is required for axonal varicosity formation. Nonetheless, currently, we still cannot rule out the potential role of other MT-binding proteins in this mechanical stress–induced varicosity formation in axons. Particularly, our results suggest that the MT-binding proteins that are similar to STOP in terms of axonal localization and sensitivity to Ca^{2+} and/or Ca^{2+}-binding proteins should be further examined in future investigations.

MT disassembly and reassembly appear to play key roles in puffing-induced initiation of axonal varicosities and recovery, respectively. During puffing-induced axonal varicosity initiation, MT disassembly is indicated by elimination of EB1-YFP plus end tracking (Fig. 8 A). At the same time, axonal transport of mitochondria and two different presynaptic proteins stopped in both directions (Fig. 8, B and C), consistent with MT disassembly. More interestingly, at the recovery stage when puffing stopped, EB1-YFP plus end tracking resumed with the same orientation (Fig. 8 A), indicating the same mechanism governing MT assembly and reassembly. Could those newly reassembled MTs support axonal transport in both anterograde and retrograde directions? The answer is yes. Detailed analysis revealed that there are some differences between original MTs and reassembled MTs in MT dynamics and axonal transport velocity, distance, and frequency (Fig. 8, D–F), which may result from modification by Ca^{2+} signaling. Nonetheless, during puffing, MT disassembly may disrupt general axonal transport and lead to accumulation of axonal cargos, resulting at least

partially in varicosity formation. During recovery after puffing, active transport may help to remove those accumulated contents and reduce varicosities.

The neurophysiological effects of concussion or subconcussion are normally immediately felt, consistent with our results that axonal varicosity formation can initiate action potentials that antidromically propagate back to soma (Fig. 9). This is different from the situation during axotomy, where axon–soma communication is mediated by retrograde Ca^{2+} waves at a speed of ∼10 µm/s (Cho et al., 2013; Rishal and Fainzilber, 2014). With the speed of Ca^{2+} waves, it will take ∼30 s for signals to reach soma along a 300-µm-long axon. This would be too slow for the onset of neurophysiological effects after mechanical impact. It is important to note that Ca^{2+} increases in axonal varicosities are more persistent and highly localized (Fig. 5), consistent with localized formation of axonal varicosities (Figs. 1 and S2) and different from propagating Ca^{2+} waves. However, in contrast with the reliable induction of axonal varicosities, rapid antidromic action potentials could only be recorded in ∼30% of the neurons (Fig. 9). The variation may be caused by the location of axonal varicosity formation, where the amount of Nav channels available for generation of action potentials varies. As we know, efficient generation of action potentials normally occurs at the AIS, a unique site in a neuron where the high concentration of Nav channels is unparalleled. It is much more difficult and unreliable to generate antidromic action potentials in the middle of axonal branches. Nonetheless, a neural circuit consisting of many different axons is still likely to reliably sense mechanical impact as a group. Furthermore, besides antidromic action potentials, axonal varicosity formation could also use Ca^{2+} waves and/or retrograde transport to communicate with the soma in long-term changes. Therefore, it is possible that there are multiple forms of axon–soma signaling that play a role at different stages of varicosity formation and/or in different neurons. These will be interesting research topics for future studies.

Collectively, our findings from this study provide novel mechanistic insights into the initial stage of a newly recognized axonal plasticity in health and disease. This process, which is still poorly characterized, may play a key role in neural development, CNS function in adults, chronic brain disorders, and various acute brain injuries.

Materials and methods

cDNA plasmids

EB1-YFP was previously described (Gu et al., 2006; Gu and Gu, 2010; Barry et al., 2014). YFP-MAP2 was made by subcloning the MAP2 cDNA into the pEYFP-N1 vector (Takara Bio Inc.). Mito-YFP was purchased from Takara Bio Inc. NSTOP-GFP was provided by C. Bosc and A. Andrieux (University Grenoble Alpes, Grenoble, France). TRPV4 was a gift from B.M. Spiegelman and L. Ye (Harvard University, Cambridge, MA). TRPV1 was purchased from OpenBiosystem. All constructs were confirmed by sequencing.

Rat hippocampal neuron culture and transfection

All animal experiments were conducted in accordance with the National Institutes of Health Animal Use Guidelines and the Institutional Animal Care and Use Committee of the Ohio State University. Hippocampal neuron culture was prepared from rat embryos at E18 as previously described (Xu et al., 2007, 2010). Rat tail collagen and poly-D-lysine were used to coat glass coverslips for neuron culture. In brief, 2 d after neuron plating, 1 µM cytosine arabinose (Sigma-Aldrich) was added to neuronal culture media to inhibit glial growth for the subsequent 2 d and then was replaced with normal neuronal culture media. Culture media were replenished twice a week by replacing half volume. For transient transfection, neurons in culture at 5–7 DIV were incubated in Opti-MEM containing 0.8 µg of cDNA plasmid and 1.5 µl of Lipofectamine 2000 (Invitrogen) for 20 min at 37°C. For old neuron (14–28 DIV) transfection, the Ca^{2+}-phosphate method was used, which was previously described (Barry et al., 2014). The neurons (21 DIV) were incubated with the calcium phosphate–cDNA mixture containing 1 µg of cDNA plasmid and 3.1 µl $CaCl_2$ (2 M) for 45–60 min at 37°C and then the medium was replaced by 10% CO_2 preequilibrated mixture of half-volume original medium plus 30% volume fresh medium (Barry et al., 2014).

Fluid micromechanical pressure provided by local puffing

To induce axonal varicosities by local puffing, the glass pipette (tip diameter ∼50 µm) was connected to a syringe via tubing filled with 5 ml Hank's buffer or other solutions. The buffer was pushed to axons or dendrites by gravity. The vertical distance between the pipette tip and cultured neurons was set at 0.4 mm. When the 190 mmH_2O pressure was applied, axonal varicosities were reliably induced. The formation of axonal swelling was considered a varicosity when it was ∼200% width of its adjacent axonal shafts. The onset time was defined as the time for an axonal segment to reach 10 varicosities per 100-µm length during puffing. It is important to note that, whereas the diameter of a varicosity increased during puffing, the diameter of its adjacent axonal shafts decreased to smaller than the diameter of normal axonal shafts before puffing (Fig. 4, I–K). Moreover, under normal conditions without puffing, no varicosity can be detected in proximal axons, but diameters of middle and distal axons are not perfectly uniform, sometimes containing a low level of varicosities. Therefore, the baseline of varicosity density in middle and distal axons was not absolute zero. These data are reflected in quantification of varicosity results.

Measurement of the fluid micromechanical pressure

The actual loading pressure exerted on neurons was determined with a microfabricated silicone membrane (500 µm in diameter and 50 µm thick) under the same experimental setup. Arrays of microdots (4 µm in diameter and 10 µm apart from center to center) were patterned on the top surface of the membrane for tracking the membrane deflection (Wang et al., 2013) under the puffing area (Fig. S1). Upon loading driven by 190 mmH_2O gravity, the mean center deflection of the membrane was measured as $w = -3.143 \pm 0.69$ µm (mean ± SD; $n = 6$). According to the linear fit of differential pressure versus center deflection of the membrane ($p = -0.798w$; $|w| \leq 12$ µm; $R^2 = 0.9997$; unit of p: mbar), the corresponding pressure was $P = 2.51 \pm 0.55$ mbar $= 0.25 \pm 0.06$ nN/µm^2.

Live-cell time-lapse imaging

Neurons growing on 25-mm coverslips were loaded into the imaging chamber (Molecular Devices) and incubated with Hank's buffer or other modified buffers at room temperature. The time-lapse imaging setup was built on an inverted microscope (TE2000; Nikon). Images were captured with a charge-coupled device camera (CoolSNAP HQ; Photometrics) through YFP or other filter sets with 1-s exposure time. The filters were changed through filter wheels controlled via Lambda 10–3 (Sutter Instrument) by MetaMorph software (Molecular Devices). Time-lapse imaging was performed with indicated intervals for hundreds of frames. This procedure was described in previous studies (Gu and Gu, 2010; Barry et al., 2014). To localize endogenous TRPV4 channels to axonal

segments that are sensitive to puffing, we initially loaded cultured hippocampal neurons (7 DIV) with 2 µM calcien AM (Thermo Fisher Scientific) in neuron culture medium at 37°C for 30 min. The neurons were washed twice and incubated with Hank's buffer at room temperature for the puffing assay and time-lapse imaging. Immediately after clear induction of axonal varicosities, the neurons were fixed with 4% formaldehyde in PBS and stained with the anti-TRPV4 antibody (see the Antibodies and immunofluorescence staining section for more details).

Solutions with different ionic components

The Hank's buffer, pH 7.4, contained 150 mM NaCl, 4 mM KCl, 1.2 mM $MgCl_2$, 1 mM $CaCl_2$, 10 mg/ml glucose, and 20 mM Hepes. The Ca^{2+}-free buffer, pH 7.4, was made by removing $CaCl_2$ and adding 2 mM EGTA. The Mg^{2+}-free buffer, pH 7.4, was made by removing $MgCl_2$. The Na^+-free buffer, pH 7.4, was made by replacing NaCl with equal molar of NMDG (Sigma-Aldrich). The Ca^{2+}- and Na^+-free buffer, pH 7.4, was made by removing $CaCl_2$, adding 2 mM EGTA, and replacing NaCl with equal molar NMDG.

Repetitive closed-skull TBI model using Thy1-YFP transgenic mice

The detailed procedure was previously described (Shitaka et al., 2011). In brief, male C57BL/6J and Thy1-YFP transgenic mice (6 wk old; n = 10; from The Jackson Laboratory) were anesthetized with 5% isoflurane and placed in a stereotaxic frame with rounded Kopf head holders (David Kopf Instruments). Temperature was controlled at 37°C using a feedback temperature controller (Cell Microcontrols). Isoflurane was delivered by nose cone at 2% in air. The heads were shaved and prepared with Betadine. A midline skin incision was made, and the skull was exposed. A rubber tip (Precision Associates, Inc.) was mounted on an electromagnetic stereotaxic impact device. The deformation of the rubber tip spread the impact force over the skull. There were <3% skull fractures and no immediate fatalities after these injuries. Mice with skull fractures were killed and were not used in any experiments, and mice with hemorrhages were excluded from the analyses. After 24 ± 1 h, a second identical closed-skull TBI procedure was performed and then mice were immediately perfused and fixed. For sham injuries, the same procedure was performed, except the impact device was discharged in the air; the handling of the mice and duration of anesthesia were the same for TBI and sham procedures. Impacts and staining procedures were performed in a blinded fashion.

Brain tissue fixation, sectioning, and immunostaining

The procedures of cardiac perfusion, fixation, sectioning, staining, and imaging were described in our previous papers (Jukkola et al., 2012, 2013; Barry et al., 2013, 2014). In brief, animals were anesthetized with 250 mg/kg avertin (Sigma-Aldrich). After cardiac perfusion and fixation, the brain was removed and postfixed in 4% formaldehyde in PBS for 1 h. The brain was cut into 3-mm blocks using an acrylic brain matrix (Braintree Scientific) and placed in 30% sucrose for at least 24 h before sectioning. The brain was arranged in the same block, embedded in optimal cutting temperature media (Sakura Finetek USA, Inc.), and stored at −80°C until sectioning. The tissue blocks were cut with a Microm HM550 cryostat (Thermo Fisher Scientific), and the 40-µm sections were collected on Superfrost Plus microscope slides (Thermo Fisher Scientific) for storage at −20°C. After immunostaining, all sections were coverslipped using tris-buffered Fluoro-Gel mounting media (Electron Microscopy Sciences).

Drug treatment

LatA, RN-1734, and GSK1016790a (GSK) from Sigma-Aldrich and Noco from EMD Millipore were prepared in DMSO. L-Glutamate and gadolinium from Sigma-Aldrich and glycine from Thermo Fisher Scientific were prepared in double-distilled H_2O. Capsaicin (Sigma-Aldrich) was dissolved in ethanol. All stock solutions were kept at −20°C and then were added to neuron culture media during treatment (<0.1% DMSO) or were freshly diluted in Hank's buffer during puffing or perfusion. To analyze the potential role of cytoskeletal proteins, neurons were treated with 10 µg/ml Noco for up to 60 min or with 2.5 µM LatA for 2 h at 37°C. 1 µM capsaicin or 0.5 µM GSK was perfused to HEK293 cells transfected with TRPV1 or TRPV4 channels, respectively, to induce channel currents via a glass pipette (tip diameter ∼50 µm).

Expression of TRP channels in HEK293 cells and voltage-clamp recording

Whole-cell voltage-clamp recording was performed on transfected HEK293 cells at room temperature (∼25°C) as described previously (Gu et al., 2012, 2013). Glass micropipettes with a resistance of ∼2–3 MΩ were pulled with a Model P-1000 Flaming/Brown micropipette puller (Sutter Instrument) and filled with the internal solution containing 122 mM $KMeSO_4$, 20 mM NaCl, 5 mM Mg-ATP, 0.3 mM GTP, and 10 mM Hepes, pH 7.2. The external solution was Hank's buffer. The whole-cell access resistance was ∼2–3 MΩ. Cells with higher access resistance were discarded. The compensation for series resistance was set at >60%. The recording was done using an Axopatch 200B amplifier, a Digidata 1440A, and pCLAMP10 software (Molecular Devices). Currents were filtered at 5 kHz. Membrane potentials of isolated cells were normally held at −80 mV.

TRPV4 siRNA knockdown

Stealth RNAi TRPV4 siRNA (ID: RSS330372) targeting to nucleotides 1,322–1,346 of rat TRPV4 (GenBank accession number NM_023970) was purchased from Invitrogen (Benfenati et al., 2011). The stock solution of double-strained siRNA was made in RNase-free water according to the instructions of the manufacturer and stored at −20°C. Scrambled siRNA was used as a negative control. Plasmid DNA (YFP) and siRNA were cotransfected into cultured neurons using Lipofectamine 2000. In brief, neurons in culture media without antibiotics at 4–5 DIV were incubated in Opti-MEM containing 20 pmol siRNA, 0.8 µg of YFP plasmid, and 1.5 µl of Lipofectamine 2000 for 20 min at 37°C. The neurons were used for live-cell time-lapse imaging or immunostaining 4–5 d after transfection.

Antibodies and immunofluorescence staining

Antibodies used in this study include rabbit polyclonal anti-TRPV4 (Lifespan Biosciences, Inc.), mouse anti-TRPV1 antibody (clone N221/17; NeuroMAB), mouse anti-STOP antibody (Cell Signaling Technology), mouse anti-β-tubulin (EMD Millipore), mouse anti-MAP2, rabbit anti-Tau1, rat anti-MBP antibodies (EMD Millipore), and Cy2- and Cy5-conjugated secondary antibodies (Jackson ImmunoResearch Laboratories, Inc.). In particular, the anti-TRPV4 antibody (LS-C94498; Lifespan Biosciences) was extensively validated by using Western blots and immunostaining of wild-type and TRPV4-null mice (as well as TRPV4 cDNA; Ryskamp et al., 2011). The procedure of immunocytochemistry was previously described (Jukkola et al., 2012, 2013). In brief, neurons were fixed with 4% formaldehyde (10% ultrapure EM grade and methanol free; Polysciences, Inc.) and 4% sucroseq in PBS for 20 min and then stained with specified antibodies under permeabilized conditions in the presence of 0.2% Triton X-100 to label total proteins. To distinguish axons and dendrites of neurons, the anti-MAP2 (a dendritic marker) antibody was used in costaining.

Ca^{2+} imaging with Fluo-4 AM on hippocampal neurons under puffing

Cultured hippocampal neurons at 7 DIV were loaded with 5 µM Fluo-4 AM (Thermo Fisher Scientific) in neuron culture medium at 37°C for

30 min. The neurons were washed twice and incubated in the Hank's buffer for the puffing assay and time-lapse imaging. The neurons were imaged continuously with the exposure time for each image at 0.5 s. Images were quantified with MetaMorph software.

Western blotting analysis for endogenous protein expression

Mice were killed with carbon dioxide, and brain and spinal cord tissues were immediately removed, flash-frozen in liquid nitrogen, and stored at −80°C until use. Tissue samples were weighed and then homogenized in 1:4 (wt/vol) Laemmli sample buffer (Bio-Rad Laboratories) with 5% β-mercaptoethanol (Sigma-Aldrich). Protein samples were resolved by SDS-PAGE and transferred to a PVDF membrane (GE Healthcare) for Western blotting, which was described previously (Barry et al., 2014). The β-tubulin level was used as control.

TEM

Monolayer primary hippocampal neurons were fixed with 4% paraformaldehyde and 3% glutaraldehyde in 0.1 M phosphate buffer, pH 7.4. Embedding, sectioning, and imaging with TEM were done in the Campus Microscopy and Imaging facility at The Ohio State University as described previously (Gardner et al., 2012).

STOP siRNA knockdown in mouse hippocampal neurons

Mouse hippocampal neurons were cultured from hippocampi of wild-type C57BL/6 mouse pups at P0–P1 with the same culture method as the rat embryonic neuron culture. Stealth RNAi, or STOP (or MAP6) siRNA (ID: MSS275832; sequence 5′-CCAAUAAGCCCAGUGCAG CGGACAA-3′) targeting mouse STOP, was purchased from Thermo Fisher Scientific. This siRNA probe was validated and successfully used in a recent study (Deloulme et al., 2015).

Simultaneous recording of action potentials and imaging of axonal varicosity initiation induced by puffing

The current-clamp recording procedure was described previously (Gu et al., 2012). The same internal solution and Hank's buffer were used for recording action potentials from primary cultured neurons. Action potentials were recorded from the neuronal soma, whereas its axons >300 µm away were puffed for the induction of varicosities imaged with time-lapse imaging at the same time. The membrane resistance, capacitance, and resting membrane potential were measured from these neurons.

Statistical analysis

Results are presented as means ± SEM. A two-tailed Student's *t* test was used for comparisons between two groups. One-way ANOVA followed by Dunnett's test was used for comparing two or more groups to one control group. *, $P < 0.05$ and **, $P < 0.01$ were considered statistically significant.

Online supplemental material

Fig. S1 shows the effect and strength of micromechanical pressure. Fig. S2 shows that puffing-induced varicosity formation depends on the age and subcellular compartment of neurons. Fig. S3 shows identification of MS ion channels responsible for puffing-induced varicosity formation in axons. Fig. S4 shows TRPV4 expression in hippocampal neurons at different developmental stages. Fig. S5 shows the development-dependent expression and localization of STOP in cultured hippocampal neurons. Fig. S6 shows how alterations of Nav channels and/or AnkG at the AIS do not affect the AIS's resistance to puffing-induced varicosity formation. Video 1 shows how puffing induced rapid and reversible varicosity formation in axons of young neurons expressing YFP. Video 2 shows how puffing induced varicosity formation in axons but not in dendrites or dendritic spines of mature neurons expressing YFP. Video 3 shows a low magnification view of puffing (by normal Hank's buffer) induced rapid and reversible varicosity formation in axons of young neurons expressing YFP. Video 4 shows how puffing with the buffer containing no Ca^{2+} and Na^{+} failed to induce varicosities in axons of young neurons expressing YFP. Video 5 shows how stimulating NMDA receptors with Glu and Gly induced varicosity formation along dendrites but not axons of mature neurons over time. Video 6 shows how puffing induced persistent Ca^{2+} increase within varicosities along an axonal segment. Video 7 shows how puffing induced a transient Ca^{2+} increase in a dendrite.

Acknowledgments

We thank Drs. Bruce M. Spiegelman, Christophe Bosc, and Annie Andrieux for cDNA constructs, the Campus Microscopy and Imaging facility at The Ohio State University for technical assistance in TEM, and Drs. Stuart Mangel, Annie Andrieux, and Jacques Brocard for commenting on the manuscript at various stages. All animal experiments have been conducted in accordance with the National Institutes of Health Animal Use Guidelines.

This work was supported in part by grants from National Institutes of Health (R01NS062720, R01NS093073, and R21AA024873) to C. Gu.

The authors declare no competing financial interests.

Author contributions: C. Gu designed and supervised the research. Y. Gu, P. Jukkola, and C. Gu performed experiments, analyzed data, and made figures. Q. Wang and Y. Zhao performed the measurement of micromechanical forces. T. Esparza and D. Brody performed the repetitive closed-skull TBI model. C. Gu wrote the manuscript.

Submitted: 13 June 2016
Revised: 17 January 2017
Accepted: 20 April 2017

References

Akhmanova, A., and M.O. Steinmetz. 2008. Tracking the ends: a dynamic protein network controls the fate of microtubule tips. *Nat. Rev. Mol. Cell Biol.* 9:309–322. http://dx.doi.org/10.1038/nrm2369

Amack, J.D., and M.L. Manning. 2012. Knowing the boundaries: Extending the differential adhesion hypothesis in embryonic cell sorting. *Science.* 338:212–215. http://dx.doi.org/10.1126/science.1223953

Andrieux, A., P.A. Salin, M. Vernet, P. Kujala, J. Baratier, S. Gory-Fauré, C. Bosc, H. Pointu, D. Proietto, A. Schweitzer, et al. 2002. The suppression of brain cold-stable microtubules in mice induces synaptic defects associated with neuroleptic-sensitive behavioral disorders. *Genes Dev.* 16:2350–2364. http://dx.doi.org/10.1101/gad.223302

Árnadóttir, J., and M. Chalfie. 2010. Eukaryotic mechanosensitive channels. *Annu. Rev. Biophys.* 39:111–137. http://dx.doi.org/10.1146/annurev.biophys.37.032807.125836

Baas, P.W., A.N. Rao, A.J. Matamoros, and L. Leo. 2016. Stability properties of neuronal microtubules. *Cytoskeleton (Hoboken).* 73:442–460.

Barry, J., M. Xu, Y. Gu, A.W. Dangel, P. Jukkola, C. Shrestha, and C. Gu. 2013. Activation of conventional kinesin motors in clusters by Shaw voltage-gated K^{+} channels. *J. Cell Sci.* 126:2027–2041. http://dx.doi.org/10.1242/jcs.122234

Barry, J., Y. Gu, P. Jukkola, B. O'Neill, H. Gu, P.J. Mohler, K.T. Rajamani, and C. Gu. 2014. Ankyrin-G directly binds to kinesin-1 to transport voltage-gated Na^{+} channels into axons. *Dev. Cell.* 28:117–131. http://dx.doi.org/10.1016/j.devcel.2013.11.023

Barsukova, A.G., M. Forte, and D. Bourdette. 2012. Focal increases of axoplasmic Ca^{2+}, aggregation of sodium–calcium exchanger, N-type Ca^{2+} channel, and actin define the sites of spheroids in axons undergoing oxidative stress. *J. Neurosci.* 32:12028–12037. http://dx.doi.org/10.1523/JNEUROSCI.0408-12.2012

Benfenati, V., M. Caprini, M. Dovizio, M.N. Mylonakou, S. Ferroni, O.P. Ottersen, and M. Amiry-Moghaddam. 2011. An aquaporin-4/transient receptor

potential vanilloid 4 (AQP4/TRPV4) complex is essential for cell-volume control in astrocytes. *Proc. Natl. Acad. Sci. USA.* 108:2563–2568. http://dx.doi.org/10.1073/pnas.1012867108

Bentley, M., and G. Banker. 2016. The cellular mechanisms that maintain neuronal polarity. *Nature.* 17:611–622.

Betz, T., D. Koch, Y.B. Lu, K. Franze, and J.A. Käs. 2011. Growth cones as soft and weak force generators. *Proc. Natl. Acad. Sci. USA.* 108:13420–13425. http://dx.doi.org/10.1073/pnas.1106145108

Beyder, A., J.L. Rae, C. Bernard, P.R. Strege, F. Sachs, and G. Farrugia. 2010. Mechanosensitivity of $Na_v1.5$, a voltage-sensitive sodium channel. *J. Physiol.* 588:4969–4985. http://dx.doi.org/10.1113/jphysiol.2010.199034

Bosc, C., J.D. Cronk, F. Pirollet, D.M. Watterson, J. Haiech, D. Job, and R.L. Margolis. 1996. Cloning, expression, and properties of the microtubule-stabilizing protein STOP. *Proc. Natl. Acad. Sci. USA.* 93:2125–2130. http://dx.doi.org/10.1073/pnas.93.5.2125

Bu, W., and L.K. Su. 2001. Regulation of microtubule assembly by human EB1 family proteins. *Oncogene.* 20:3185–3192. http://dx.doi.org/10.1038/sj.onc.1204429

Campàs, O., T. Mammoto, S. Hasso, R.A. Sperling, D. O'Connell, A.G. Bischof, R. Maas, D.A. Weitz, L. Mahadevan, and D.E. Ingber. 2014. Quantifying cell-generated mechanical forces within living embryonic tissues. *Nat. Methods.* 11:183–189. http://dx.doi.org/10.1038/nmeth.2761

Caterina, M.J., M.A. Schumacher, M. Tominaga, T.A. Rosen, J.D. Levine, and D. Julius. 1997. The capsaicin receptor: a heat-activated ion channel in the pain pathway. *Nature.* 389:816–824. http://dx.doi.org/10.1038/39807

Cho, Y., R. Sloutsky, K.M. Naegle, and V. Cavalli. 2013. Injury-induced HDAC5 nuclear export is essential for axon regeneration. *Cell.* 155:894–908. (published erratum appears in *Cell*. 2015. 161:691) http://dx.doi.org/10.1016/j.cell.2013.10.004

Christensen, A.P., and D.P. Corey. 2007. TRP channels in mechanosensation: direct or indirect activation? *Nature.* 8:510–521.

Chung, R.S., J.A. Staal, G.H. McCormack, T.C. Dickson, M.A. Cozens, J.A. Chuckowree, M.C. Quilty, and J.C. Vickers. 2005. Mild axonal stretch injury in vitro induces a progressive series of neurofilament alterations ultimately leading to delayed axotomy. *J. Neurotrauma.* 22:1081–1091. http://dx.doi.org/10.1089/neu.2005.22.1081

Cosens, D.J., and A. Manning. 1969. Abnormal electroretinogram from a *Drosophila* mutant. *Nature.* 224:285–287. http://dx.doi.org/10.1038/224285a0

Couégnas, A., A. Schweitzer, A. Andrieux, M.S. Ghandour, and N. Boehm. 2007. Expression pattern of STOP lacZ reporter gene in adult and developing mouse brain. *J. Neurosci. Res.* 85:1515–1527. http://dx.doi.org/10.1002/jnr.21278

Debanne, D. 2004. Information processing in the axon. *Nat. Rev. Neurosci.* 5:304–316. http://dx.doi.org/10.1038/nrn1397

DeFord, S.M., M.S. Wilson, A.C. Rice, T. Clausen, L.K. Rice, A. Barabnova, R. Bullock, and R.J. Hamm. 2002. Repeated mild brain injuries result in cognitive impairment in B6C3F1 mice. *J. Neurotrauma.* 19:427–438. http://dx.doi.org/10.1089/08977150252932389

Delmas, P., J. Hao, and L. Rodat-Despoix. 2011. Molecular mechanisms of mechanotransduction in mammalian sensory neurons. *Nat. Rev. Neurosci.* 12:139–153. http://dx.doi.org/10.1038/nrn2993

Deloulme, J.C., S. Gory-Fauré, F. Mauconduit, S. Chauvet, J. Jonckheere, B. Boulan, E. Mire, J. Xue, M. Jany, C. Maucler, et al. 2015. Microtubule-associated protein 6 mediates neuronal connectivity through Semaphorin 3E-dependent signalling for axonal growth. *Nat. Commun.* 6:7246. http://dx.doi.org/10.1038/ncomms8246

Eastwood, S.L., L. Lyon, L. George, A. Andrieux, D. Job, and P.J. Harrison. 2007. Altered expression of synaptic protein mRNAs in STOP (MAP6) mutant mice. *J. Psychopharmacol. (Oxford).* 21:635–644. http://dx.doi.org/10.1177/0269881106068825

Elkin, B.S., E.U. Azeloglu, K.D. Costa, and B. Morrison III. 2007. Mechanical heterogeneity of the rat hippocampus measured by atomic force microscope indentation. *J. Neurotrauma.* 24:812–822. http://dx.doi.org/10.1089/neu.2006.0169

Engler, A.J., S. Sen, H.L. Sweeney, and D.E. Discher. 2006. Matrix elasticity directs stem cell lineage specification. *Cell.* 126:677–689. http://dx.doi.org/10.1016/j.cell.2006.06.044

Fournet, V., A. Schweitzer, C. Chevarin, J.C. Deloulme, M. Hamon, B. Giros, A. Andrieux, and M.P. Martres. 2012. The deletion of STOP/MAP6 protein in mice triggers highly altered mood and impaired cognitive performances. *J. Neurochem.* 121:99–114. http://dx.doi.org/10.1111/j.1471-4159.2011.07615.x

Franze, K., J. Gerdelmann, M. Weick, T. Betz, S. Pawlizak, M. Lakadamyali, J. Bayer, K. Rillich, M. Gögler, Y.B. Lu, et al. 2009. Neurite branch retraction is caused by a threshold-dependent mechanical impact. *Biophys. J.* 97:1883–1890. http://dx.doi.org/10.1016/j.bpj.2009.07.033

Gao, X., P. Deng, Z.C. Xu, and J. Chen. 2011. Moderate traumatic brain injury causes acute dendritic and synaptic degeneration in the hippocampal dentate gyrus. *PLoS One.* 6:e24566. http://dx.doi.org/10.1371/journal.pone.0024566

Gardner, A., P. Jukkola, and C. Gu. 2012. Myelination of rodent hippocampal neurons in culture. *Nat. Protoc.* 7:1774–1782. http://dx.doi.org/10.1038/nprot.2012.100

Gibson, H.E., J.G. Edwards, R.S. Page, M.J. Van Hook, and J.A. Kauer. 2008. TRPV1 channels mediate long-term depression at synapses on hippocampal interneurons. *Neuron.* 57:746–759. http://dx.doi.org/10.1016/j.neuron.2007.12.027

Gilmour, D., H. Knaut, H.M. Maischein, and C. Nüsslein-Volhard. 2004. Towing of sensory axons by their migrating target cells in vivo. *Nat. Neurosci.* 7:491–492. http://dx.doi.org/10.1038/nn1235

Grevesse, T., B.E. Dabiri, K.K. Parker, and S. Gabriele. 2015. Opposite rheological properties of neuronal microcompartments predict axonal vulnerability in brain injury. *Sci. Rep.* 5:9475. http://dx.doi.org/10.1038/srep09475

Gu, Y., and C. Gu. 2010. Dynamics of Kv1 channel transport in axons. *PLoS One.* 5:e11931. http://dx.doi.org/10.1371/journal.pone.0011931

Gu, Y., and C. Gu. 2014. Physiological and pathological functions of mechanosensitive ion channels. *Mol. Neurobiol.* 50:339–347. http://dx.doi.org/10.1007/s12035-014-8654-4

Gu, C., W. Zhou, M.A. Puthenveedu, M. Xu, Y.N. Jan, and L.Y. Jan. 2006. The microtubule plus-end tracking protein EB1 is required for Kv1 voltage-gated K^+ channel axonal targeting. *Neuron.* 52:803–816. http://dx.doi.org/10.1016/j.neuron.2006.10.022

Gu, Y., J. Barry, R. McDougel, D. Terman, and C. Gu. 2012. Alternative splicing regulates kv3.1 polarized targeting to adjust maximal spiking frequency. *J. Biol. Chem.* 287:1755–1769. http://dx.doi.org/10.1074/jbc.M111.299305

Gu, Y., J. Barry, and C. Gu. 2013. Kv3 channel assembly, trafficking and activity are regulated by zinc through different binding sites. *J. Physiol.* 591:2491–2507. http://dx.doi.org/10.1113/jphysiol.2013.251983

Guillaud, L., C. Bosc, A. Fourest-Lieuvin, E. Denarier, F. Pirollet, L. Lafanechère, and D. Job. 1998. STOP proteins are responsible for the high degree of microtubule stabilization observed in neuronal cells. *J. Cell Biol.* 142:167–179. http://dx.doi.org/10.1083/jcb.142.1.167

Harrington, A.W., and D.D. Ginty. 2013. Long-distance retrograde neurotrophic factor signalling in neurons. *Nat. Rev. Neurosci.* 14:177–187. http://dx.doi.org/10.1038/nrn3253

Hasbani, M.J., M.L. Schlief, D.A. Fisher, and M.P. Goldberg. 2001. Dendritic spines lost during glutamate receptor activation reemerge at original sites of synaptic contact. *J. Neurosci.* 21:2393–2403.

Hemphill, M.A., B.E. Dabiri, S. Gabriele, L. Kerscher, C. Franck. J.A. Goss, P.W. Alford, and K.K. Parker. 2011. A possible role for integrin signaling in diffuse axonal injury. *PLoS One.* 6:e22899 http://dx.doi.org/10.1371/journal.pone.0022899

Iwata, A., P.K. Stys, J.A. Wolf, X.H. Chen, A.G. Taylor, D.F. Meaney, and D.H. Smith. 2004. Traumatic axonal injury induces proteolytic cleavage of the voltage-gated sodium channels modulated by tetrodotoxin and protease inhibitors. *J. Neurosci.* 24:4605–4613. http://dx.doi.org/10.1523/JNEUROSCI.0515-03.2004

Jukkola, P.I., A.E. Lovett-Racke, S.S. Zamvil, and C. Gu. 2012. K^+ channel alterations in the progression of experimental autoimmune encephalomyelitis. *Neurobiol. Dis.* 47:280–293. http://dx.doi.org/10.1016/j.nbd.2012.04.012

Jukkola, P., T. Guerrero, V. Gray, and C. Gu. 2013. Astrocytes differentially respond to inflammatory autoimmune insults and imbalances of neural activity. *Acta Neuropathol. Commun.* 1:70. http://dx.doi.org/10.1186/2051-5960-1-70

Kanayama, G., M. Takeda, H. Niigawa, Y. Ikura, H. Tamii, N. Taniguchi, T. Kudo, Y. Miyamae, T. Morihara, and T. Nishimura. 1996. The effects of repetitive mild brain injury on cytoskeletal protein and behavior. *Methods Find. Exp. Clin. Pharmacol.* 18:105–115.

Kang, J.S., J.H. Tian, P.Y. Pan, P. Zald, C. Li, C. Deng, and Z.H. Sheng. 2008. Docking of axonal mitochondria by syntaphilin controls their mobility and affects short-term facilitation. *Cell.* 132:137–148. http://dx.doi.org/10.1016/j.cell.2007.11.024

Koleske, A.J. 2013. Molecular mechanisms of dendrite stability. *Nature.* 14:536–550.

Laurer, H.L., F.M. Bareyre, V.M. Lee, J.Q. Trojanowski, L. Longhi, R. Hoover, K.E. Saatman, R. Raghupathi, S. Hoshino, M.S. Grady, and T.K. McIntosh. 2001. Mild head injury increasing the brain's vulnerability to a second

concussive impact. *J. Neurosurg.* 95:859–870. http://dx.doi.org/10.3171/jns.2001.95.5.0859

Lefèvre, J., K.G. Chernov, V. Joshi, S. Delga, F. Toma, D. Pastré, P.A. Curmi, and P. Savarin. 2011. The C terminus of tubulin, a versatile partner for cationic molecules: Binding of Tau, polyamines, and calcium. *J. Biol. Chem.* 286:3065–3078. http://dx.doi.org/10.1074/jbc.M110.144089

Liedtke, W., and J.M. Friedman. 2003. Abnormal osmotic regulation in *trpv4*$^{-/-}$ mice. *Proc. Natl. Acad. Sci. USA.* 100:13698–13703. http://dx.doi.org/10.1073/pnas.1735416100

Liedtke, W., Y. Choe, M.A. Martí-Renom, A.M. Bell, C.S. Denis, A. Sali, A.J. Hudspeth, J.M. Friedman, and S. Heller. 2000. Vanilloid receptor-related osmotically activated channel (VR-OAC), a candidate vertebrate osmoreceptor. *Cell.* 103:525–535. http://dx.doi.org/10.1016/S0092-8674(00)00143-4

Ligon, L.A., S.S. Shelly, M. Tokito, and E.L. Holzbaur. 2003. The microtubule plus-end proteins EB1 and dynactin have differential effects on microtubule polymerization. *Mol. Biol. Cell.* 14:1405–1417. http://dx.doi.org/10.1091/mbc.E02-03-0155

Lu, Y.B., K. Franze, G. Seifert, C. Steinhäuser, F. Kirchhoff, H. Wolburg, J. Guck, P. Janmey, E.Q. Wei, J. Käs, and A. Reichenbach. 2006. Viscoelastic properties of individual glial cells and neurons in the CNS. *Proc. Natl. Acad. Sci. USA.* 103:17759–17764. http://dx.doi.org/10.1073/pnas.0606150103

Luo, L., and D.D. O'Leary. 2005. Axon retraction and degeneration in development and disease. *Annu. Rev. Neurosci.* 28:127–156. http://dx.doi.org/10.1146/annurev.neuro.28.061604.135632

Margolis, R.L., C.T. Rauch, and D. Job. 1986. Purification and assay of a 145-kDa protein (STOP145) with microtubule-stabilizing and motility behavior. *Proc. Natl. Acad. Sci. USA.* 83:639–643. http://dx.doi.org/10.1073/pnas.83.3.639

Montell, C., and G.M. Rubin. 1989. Molecular characterization of the drosophila trp locus: A putative integral membrane protein required for phototransduction. *Neuron.* 2:1313–1323. http://dx.doi.org/10.1016/0896-6273(89)90069-X

Morris, C.E., and P.F. Juranka. 2007. Nav channel mechanosensitivity: Activation and inactivation accelerate reversibly with stretch. *Biophys. J.* 93:822–833. http://dx.doi.org/10.1529/biophysj.106.101246

Namba, T., Y. Funahashi, S. Nakamuta, C. Xu, T. Takano, and K. Kaibuchi. 2015. Extracellular and intracellular signaling for neuronal polarity. *Physiol. Rev.* 95:995–1024. http://dx.doi.org/10.1152/physrev.00025.2014

Nikić, I., D. Merkler, C. Sorbara, M. Brinkoetter, M. Kreutzfeldt, F.M. Bareyre, W. Brück, D. Bishop, T. Misgeld, and M. Kerschensteiner. 2011. A reversible form of axon damage in experimental autoimmune encephalomyelitis and multiple sclerosis. *Nat. Med.* 17:495–499. http://dx.doi.org/10.1038/nm.2324

Pirollet, F., J. Derancourt, J. Haiech, D. Job, and R.L. Margolis. 1992. Calcium-calmodulin regulated effectors of microtubule stability in bovine brain. *Biochemistry.* 31:8849–8855. http://dx.doi.org/10.1021/bi00152a022

Reeves, T.M., L.L. Phillips, and J.T. Povlishock. 2005. Myelinated and unmyelinated axons of the corpus callosum differ in vulnerability and functional recovery following traumatic brain injury. *Exp. Neurol.* 196:126–137. http://dx.doi.org/10.1016/j.expneurol.2005.07.014

Richard, M., J. Sacquet, M. Jany, A. Schweitzer, F. Jourdan, A. Andrieux, and V. Pellier-Monnin. 2009. STOP proteins contribute to the maturation of the olfactory system. *Mol. Cell. Neurosci.* 41:120–134. http://dx.doi.org/10.1016/j.mcn.2009.02.004

Rishal, I., and M. Fainzilber. 2014. Axon–soma communication in neuronal injury. *Nat. Rev. Neurosci.* 15:32–42. http://dx.doi.org/10.1038/nrn3609

Ryskamp, D.A., P. Witkovsky, P. Barabas, W. Huang, C. Koehler, N.P. Akimov, S.H. Lee, S. Chauhan, W. Xing, R.C. Rentería, et al. 2011. The polymodal ion channel transient receptor potential vanilloid 4 modulates calcium flux, spiking rate, and apoptosis of mouse retinal ganglion cells. *J. Neurosci.* 31:7089–7101. http://dx.doi.org/10.1523/JNEUROSCI.0359-11.2011

Sánchez, C., J. Díaz-Nido, and J. Avila. 2000. Phosphorylation of microtubule-associated protein 2 (MAP2) and its relevance for the regulation of the neuronal cytoskeleton function. *Prog. Neurobiol.* 61:133–168. http://dx.doi.org/10.1016/S0301-0082(99)00046-5

Serrano, L., A. Valencia, R. Caballero, and J. Avila. 1986. Localization of the high affinity calcium-binding site on tubulin molecule. *J. Biol. Chem.* 261:7076–7081.

Shepherd, G.M., and K.M. Harris. 1998. Three-dimensional structure and composition of CA3→CA1 axons in rat hippocampal slices: Implications for presynaptic connectivity and compartmentalization. *J. Neurosci.* 18:8300–8310.

Shibasaki, K., M. Suzuki, A. Mizuno, and M. Tominaga. 2007. Effects of body temperature on neural activity in the hippocampus: Regulation of resting membrane potentials by transient receptor potential vanilloid 4. *J. Neurosci.* 27:1566–1575. http://dx.doi.org/10.1523/JNEUROSCI.4284-06.2007

Shitaka, Y., H.T. Tran, R.E. Bennett, L. Sanchez, M.A. Levy, K. Dikranian, and D.L. Brody. 2011. Repetitive closed-skull traumatic brain injury in mice causes persistent multifocal axonal injury and microglial reactivity. *J. Neuropathol. Exp. Neurol.* 70:551–567. http://dx.doi.org/10.1097/NEN.0b013e31821f891f

Smith, D.H., R. Hicks, and J.T. Povlishock. 2013. Therapy development for diffuse axonal injury. *J. Neurotrauma.* 30:307–323. http://dx.doi.org/10.1089/neu.2012.2825

Staal, J.A., T.C. Dickson, R.S. Chung, and J.C. Vickers. 2007. Cyclosporin-A treatment attenuates delayed cytoskeletal alterations and secondary axotomy following mild axonal stretch injury. *Dev. Neurobiol.* 67:1831–1842. http://dx.doi.org/10.1002/dneu.20552

Strotmann, R., C. Harteneck, K. Nunnenmacher, G. Schultz, and T.D. Plant. 2000. OTRPC4, a nonselective cation channel that confers sensitivity to extracellular osmolarity. *Nat. Cell Biol.* 2:695–702. http://dx.doi.org/10.1038/35036318

Tang-Schomer, M.D., V.E. Johnson, P.W. Baas, W. Stewart, and D.H. Smith. 2012. Partial interruption of axonal transport due to microtubule breakage accounts for the formation of periodic varicosities after traumatic axonal injury. *Exp. Neurol.* 233:364–372. http://dx.doi.org/10.1016/j.expneurol.2011.10.030

Tseng, C.Y., and B.L. Firestein. 2011. The role of PSD-95 and cypin in morphological changes in dendrites following sublethal NMDA exposure. *J. Neurosci.* 31:15468–15480. http://dx.doi.org/10.1523/JNEUROSCI.2442-11.2011

van Beuningen, S.F., and C.C. Hoogenraad. 2016. Neuronal polarity: remodeling microtubule organization. *Curr. Opin. Neurobiol.* 39:1–7. http://dx.doi.org/10.1016/j.conb.2016.02.003

Van Essen, D.C. 1997. A tension-based theory of morphogenesis and compact wiring in the central nervous system. *Nature.* 385:313–318. http://dx.doi.org/10.1038/385313a0

Venkatachalam, K., and C. Montell. 2007. TRP channels. *Annu. Rev. Biochem.* 76:387–417. http://dx.doi.org/10.1146/annurev.biochem.75.103004.142819

Wang, X., and T.L. Schwarz. 2009. The mechanism of Ca^{2+}-dependent regulation of kinesin-mediated mitochondrial motility. *Cell.* 136:163–174. http://dx.doi.org/10.1016/j.cell.2008.11.046

Wang, Q., X. Zhang, and Y. Zhao. 2013. Micromechanical stimulator for localized cell loading: fabrication and strain analysis. *J. Micromech. Microeng.* 23:015002. http://dx.doi.org/10.1088/0960-1317/23/1/015002

Xu, M., R. Cao, R. Xiao, M.X. Zhu, and C. Gu. 2007. The axon–dendrite targeting of Kv3 (Shaw) channels is determined by a targeting motif that associates with the T1 domain and ankyrin G. *J. Neurosci.* 27:14158–14170. http://dx.doi.org/10.1523/JNEUROSCI.3675-07.2007

Xu, M., Y. Gu, J. Barry, and C. Gu. 2010. Kinesin I transports tetramerized Kv3 channels through the axon initial segment via direct binding. *J. Neurosci.* 30:15987–16001. http://dx.doi.org/10.1523/JNEUROSCI.3565-10.2010

Yang, J., R.M. Weimer, D. Kallop, O. Olsen, Z. Wu, N. Renier, K. Uryu, and M. Tessier-Lavigne. 2013. Regulation of axon degeneration after injury and in development by the endogenous calpain inhibitor calpastatin. *Neuron.* 80:1175–1189. http://dx.doi.org/10.1016/j.neuron.2013.08.034

Zheng, Y., J. Wildonger, B. Ye, Y. Zhang, A. Kita, S.H. Younger, S. Zimmerman, L.Y. Jan, and Y.N. Jan. 2008. Dynein is required for polarized dendritic transport and uniform microtubule orientation in axons. *Nat. Cell Biol.* 10:1172–1180. http://dx.doi.org/10.1038/ncb1777

Ziv, N.E., and M.E. Spira. 1995. Axotomy induces a transient and localized elevation of the free intracellular calcium concentration to the millimolar range. *J. Neurophysiol.* 74:2625–2637.